SYSTEMATIC ANALYSIS OF 22 MICROLENSING PARALLAX CANDIDATES

Shawn Poindexter,[1] Cristina Afonso,[2] David P. Bennett,[3] Jean-Francois Glicenstein,[4]
Andrew Gould,[1] Michał K. Szymański,[5] and Andrzej Udalski[5]

ABSTRACT

We attempt to identify all microlensing parallax events for which the parallax fit improves $\Delta\chi^2 > 100$ relative to a standard microlensing model. We outline a procedure to identify three types of discrete degeneracies (including a new one that we dub the "ecliptic degeneracy") and find many new degenerate solutions in 16 previously published and six unpublished events. Only four events have one unique solution, and the other 18 events have a total of 44 solutions. Our sample includes three previously identified black hole (BH) candidates. We consider the newly discovered degenerate solutions and determine the relative likelihood that each of these is a BH. We find that the lens of event MACHO-99-BLG-22 is a strong BH candidate (78%), event MACHO-96-BLG-5 is a marginal BH candidate (37%), and MACHO-98-BLG-6 is a weak BH candidate (2.2%). The lens of event OGLE-2003-BLG-84 may be a Jupiter-mass free-floating planet candidate based on a weak $3\,\sigma$ detection of finite-source effects. We find that event MACHO-179-A is a brown dwarf candidate within ~100 pc of the Sun, mostly due to its very small projected Einstein radius, $\tilde{r}_E = 0.23 \pm 0.05$ AU. As expected, these microlensing parallax events are biased toward lenses that are heavier and closer than average. These events were examined for xallarap (or binary-source motion), which can mimic parallax. We find that 23% of these events are strongly affected by xallarap.

Subject headings: astrometry — gravitational lensing

Online material: machine-readable table

1. INTRODUCTION

Since microlens parallaxes were first predicted (Gould 1992) and observed (Alcock et al. 1995), about 20 parallax events have been reported in the literature. The microlens parallax, π_E, expresses the size of the Earth's orbit (1 AU) relative to the Einstein radius of the microlensing event projected onto the observer plane ($\tilde{r}_E$). That is, $\pi_E = \text{AU}/\tilde{r}_E$. It is related to the lens mass M and the lens-source relative parallax $\pi_{rel} = (1 \text{ AU})(1/D_L - 1/D_S)$ by

$$\pi_E = \sqrt{\frac{\pi_{rel}}{\kappa M}}, \quad \kappa = \frac{4G}{c^2 \text{ AU}} \sim 8.1 \frac{\text{mas}}{M_\odot}. \qquad (1)$$

The microlens parallax is determined by modeling the distortion in the microlensing light curve, relative to the standard (Paczyński 1986) shape, that is generated by the deviation of the Earth's motion from a straight line. Other things being equal, the bigger the parallax, the greater the distortion.

Microlens parallaxes can help break the classic timescale degeneracy in microlensing events and, because of this, they have a wide range of potential applications. For most events, the only parameter that one can measure that gives any information about the underlying physical characteristics of the lens is the Einstein

timescale t_E. This is related to M, π_{rel}, and the lens-source relative proper motion μ_{rel} by

$$t_E = \frac{\theta_E}{\mu_{rel}}, \quad \theta_E = \sqrt{\kappa M \pi_{rel}}, \qquad (2)$$

where θ_E is the angular Einstein radius. Hence, by measuring π_E, one eliminates the uncertainties arising from the unknown relative proper motion and so obtains a direct relation between M and π_{rel} through equation (1). Alcock et al. (1995) used this relation to place constraints on the lens mass and distance for the very first parallax event, and the same principle has been applied for many subsequent events. Indeed, Bennett et al. (2002), Mao et al. (2002), and Agol et al. (2002) used parallax measurements to argue that the lenses of three microlensing events were black hole (BH) candidates. Moreover, Han & Gould (1995) showed that an ensemble of parallax events could be used to constrain the mass function (MF) of the lenses.

If both π_E and θ_E are measured, one can determine both $M = \theta_E/\kappa\pi_E$ and $\pi_{rel} = \pi_E\theta_E$ (Gould 1992). To date, this has been done fairly accurately for three events (An et al. 2002; Gould 2004; Gould et al. 2004; Kubas et al. 2005) and more crudely for one other (Jiang et al. 2004).

However, microlens parallaxes are subject to their own degeneracies. To understand these, it is necessary to recognize that the microlens parallax is actually a vector quantity $\boldsymbol{\pi}_E$, whose magnitude is given by π_E and whose direction is that of the lens motion relative to the source. For relatively short microlensing events, $t_E \lesssim \text{yr}/2\pi$, the Earth's acceleration may be approximated as roughly constant during the event. Gould et al. (1994) pointed out that this would give rise to a strong asymmetry in the light curve but otherwise weak effects. Since the magnitude of this asymmetry is proportional to $\pi_{E,\parallel}$ (the component of $\boldsymbol{\pi}_E$ parallel to the Earth's acceleration), one could potentially measure this component of the vector parallax in such short events, but not the

[1] Department of Astronomy, Ohio State University, 140 West 18th Avenue, Columbus, OH 43210; sdp@astronomy.ohio-state.edu, gould@astronomy.ohio-state.edu.
[2] Max-Planck-Institut für Astronomie, Koenigstühl 17, D-69117 Heidelberg, Germany; afonso@mpia-hd.mpg.de.
[3] Department of Physics, Notre Dame University, 225 Niewland Science Hall, Notre Dame, IN 46566; bennett@nd.edu.
[4] DAPNIA-SPP, CE-Saclay, F-91191 Gif-sur-Yvette, France; glicens@hep.saclay.cea.fr.
[5] Warsaw University Observatory, Al. Ujazdowskie 4, PL-00-478 Warsaw, Poland; udalski@astrouw.edu.pl, msz@astrouw.edu.pl.

other ($\pi_{E,\perp}$). Such essentially one-dimensional parallax measurements have subsequently been made for three events (Park et al. 2004; Ghosh et al. 2004; Jiang et al. 2004).

On closer examination of this limit, Smith et al. (2003) found that even if the Earth's motion were approximated as uniformly accelerating, one could in principle determine both components of π_E. However, they noted three distinct types of degeneracies. The first is a twofold discrete degeneracy, essentially whether the lens moves on the left or right side of the source as it passes it in the plane of the sky. This degeneracy, which gives rise to relatively small changes in π_E as well as other event parameters, is known as the "constant-acceleration" degeneracy. Smith et al. (2003) showed that even though the Earth's acceleration is not perfectly uniform, the constant-acceleration degeneracy did affect a number of archival events. The second degeneracy is a continuous one between $\pi_{E,\perp}$ and blending of the light curve by light from an additional, unmagnified source. Since both of these give rise to light-curve distortions that are symmetric about the peak, they can be mistaken for each other unless the data are of sufficiently high quality. Indeed, the source flux, the background flux, the event timescale, and the event impact parameter all affect the light curve symmetrically about the peak, and disentangling these effects is a classic problem in the interpretation of microlensing events. Adding $\pi_{E,\perp}$ to the mix simply exacerbates an already difficult situation. This second degeneracy therefore leads to one-dimensional parallax measurements and is essentially the same as the one identified by Gould et al. (1994). Finally, Smith et al. (2003) noted that if the source were accelerating (due to a binary companion), it could produce exactly the same light-curve distortion as the Earth's acceleration. This degeneracy is especially severe if both accelerations can be approximated as uniform but, at least in principle, the binary orbit of the source could mimic with infinite precision the orbital parameters of the Earth. In practice, however, one would not expect a binary source to have exactly the same orbital parameters as the Earth. Hence, if the data are of sufficient quality to measure these parameters, and if the measured parameters are inconsistent with those of the Earth, this would imply that the light curve is affected by the acceleration of the source rather than the Earth. Conversely, if the fit parameters closely mimic those of the Earth, one can infer that the light-curve distortions are most likely due to parallax.

In principle, acceleration of the lens could also produce light-curve distortions that mimic parallax. However, in most cases, if the lens has a companion with a period close to a year, the light curve will be far more severely affected by the binarity of the lens than by the accelerated motion of one of its components.

To mathematically analyze the constant-acceleration degeneracy, Smith et al. (2003) Taylor expanded the lens-source separation to fourth order in time. Gould (2004) adopted this same approach but included the Earth's jerk and its acceleration. Surprisingly, this addition led to the identification of a new, so-called jerk-parallax degeneracy. In contrast to the constant-acceleration degeneracy, the jerk-parallax degeneracy can lead to radically different estimates of π_E, in both its magnitude and direction. Indeed, Gould (2004) was specifically motivated to perform this analysis by his empirical discovery of two very different parallax solutions for the event MACHO-LMC-5. These solutions led to very different mass and distance estimates for the lens, an ambiguity that was finally resolved by a direct (trigonometric) parallax measurement by Drake et al. (2004). Gould (2004) showed that his formalism, although idealized, predicted the second solution, given the first, extremely well. Moreover, Park et al. (2004) showed that this formalism also predicted the location of a sec-

ond solution in another event, giving confidence that one could indeed find additional solutions analytically if they existed.

This confidence is important because the previous practice was to search for additional parallax solutions by brute force, i.e., by starting with seed solutions at many different places in parameter space and then moving downhill on the χ^2 surface until reaching a local minimum. Although such an approach can yield additional solutions, there is no guarantee that it will find them if they exist. Indeed, we show in this paper that this brute force approach did in fact fail to find additional parallax solutions for events that were previously analyzed.

A crucial component of the Gould (2004) approach is to work in the geocentric frame, i.e., the Galilean frame that is at rest with respect to the Earth at the peak of the event. In this frame, all the parameters characterizing the event (except the parallax) are approximately the same for all solutions (up to the left-right ambiguity mentioned above). This means that searches, even when they are not guided by analytic insight, are much more likely to be successful.

Here we undertake a systematic study of all microlensing events with parallax signatures that are detected with "good confidence," which we define as a $\Delta\chi^2 > 100$ improvement relative to the standard (nonparallax) solution. We seek to identify all parallax solutions (if there are more than one) and to determine whether the event is better fitted by "xallarap" (binary-source motion) rather than parallax. We aim to achieve several interrelated goals.

First, at present it is unknown how severely parallax events are affected by discrete degeneracies. These have been systematically searched for in only four events, MACHO-LMC-5 (Gould 2004), MOA-2003-BLG-37 (Park et al. 2004), OGLE-2003-BLG-175/MOA-2003-BLG-45 (Ghosh et al. 2004), and OGLE-2003-BLG-238 (Jiang et al. 2004). None of these events satisfy $\Delta\chi^2 > 100$ and so none are in the present study. In principle, therefore, it is possible that the events that do satisfy this criterion are not seriously affected by degeneracies.

Second, by examining a large ensemble of events, we seek to identify patterns in the event degeneracies. In fact, we find a new class of degeneracy, which we dub the "ecliptic" degeneracy. As noted by Jiang et al. (2004), events lying exactly on the ecliptic will be subject to an exact twofold degeneracy. We show that this degeneracy is a combination of the previously identified constant-acceleration and jerk-parallax degeneracies. Moreover, we show that, since events seen toward the Galactic bulge are generally quite near the ecliptic, this degeneracy indeed affects many of these events.

Third, we seek to reanalyze the three BH candidates, taking account of any new degenerate solutions that we find. In particular, we calculate the relative likelihood that these events are due to main-sequence (MS) stars, white dwarfs (WDs), neutron stars (NSs), and BHs. We find that one of the three is a strong candidate, one is a very weak candidate, and one is a plausible, but not strong, candidate.

Fourth, we analyze the likelihood distributions of all events with respect to mass and distance. As has been frequently noted, parallax events are expected to be biased toward lenses that are heavier, closer, and slower than average. We confirm this expectation.

Fifth, we analyze all events for xallarap. Of events with apparent parallax signatures, for what fraction is this actually due to xallarap? Of course, the sample is somewhat biased since xallarap due to short-period binaries would not mimic parallax effects very well and so might not make our cut. Nevertheless, we expect that most xallarap events with recognizable signals will be in our sample, giving us a good probe of the relative frequency

of parallax and xallarap events. We find that 23% of our parallax candidate sample is strongly affected by xallarap.

Finally, we check our sample for any intrinsically interesting events other than the BH candidates that have been previously identified. Indeed, we find a brown dwarf candidate, which probably lies within ~100 pc of the Sun. We also find a candidate free-floating planet of mass $M \sim 10^{-3} \, M_\odot$. In all we analyze 22 events, of which 16 are taken from the literature and 6 are previously unanalyzed events from the OGLE-III database.

2. MICROLENSING PARALLAX SAMPLE

We attempt to identify all point-lens microlensing parallax events with improvements of $\Delta\chi^2 > 100$ relative to a standard (nonparallax) microlensing model.[6] To do so, we first search the literature for parallax events with published models. We identify 16 such events, including 10 discovered by MACHO[7] (Alcock et al. 1993; Bennett et al. 2002), 4 discovered by OGLE[8] (Udalski et al. 1993), 1 discovered by MOA[9] (Bond et al. 2001), and 1 discovered by EROS (Afonso et al. 2003). Some events discovered by one collaboration were simultaneously monitored by another, and we attempt to include these data sets in our analysis. Some parallax events in the literature such as MACHO-LMC-5 (Alcock et al. 1997b, 2001; Gould 2004) did not make our $\Delta\chi^2 > 100$ cut.

Bennett et al. (2002) identified nine MACHO parallax events that made our sample but did not publish their analysis of three of these because of their more severe $\Delta\chi^2$ threshold. We find that one event that they did analyze, MACHO-99-BLG-8, has $\Delta\chi^2 = 56.51$. However, we also find that the standard solution has severe negative blending (an unrealistic result) and that when the background is constrained to zero for the standard solution, $\Delta\chi^2 = 1190.27$. Similarly, we find that EROS-BLG-29 has $\Delta\chi^2 = 41.44$, but also with severe negative blending. When the blending is constrained to zero, $\Delta\chi^2 = 129.46$.

Next we search for unpublished parallax events from online data obtained by the OGLE-III (Udalski 2003) and MOA (Bond et al. 2001) collaborations among events identified up through the 2003 seasons. These events are visually examined if the geocentric timescale is $t_E \geq 60$ days. We then fit plausible parallax candidates with both standard and parallax microlensing models and adopt those with $\Delta\chi^2 \geq 100$. We find six such events, all from the OGLE-III database. The microlensing events are listed in Table 1. Most of the headings of this table are self-evident. The baseline magnitude of the event m_S is a calibrated Johnson/Cousins R for MACHO events, a calibrated Cousins I for OGLE-II events (1999 and 2000), an approximately calibrated Cousins I for OGLE-III events (2002 and 2003), an approximately calibrated Cousins I for MOA-2000-BLG-11, and a calibrated Cousins I for EROS-BLG-29. The one exception to this is event MACHO-99-BLG-22, in which the Cousins I band is given because the MACHO R band is corrupted. The column "Points" give the total number of original data points and the number removed. The renormalization factors are given in an order determined as

follows. For each event, the band(s) of the collaboration whose name is attached to the event are given first. For MACHO, there are two bands R_{MACHO} and B_{MACHO}, and these are given in this order. When there are additional bands, these are given in the order they are mentioned in § 3.5. For event MACHO-104-C we renormalize the errors separately for the peak and baseline (displayed on the left and right sides of a solidus, respectively).

3. PARALLAX SOLUTIONS

We first fit each event to a standard Paczyński (1986) curve,

$$F_i(t) = f_{s,i} A[u(t)] + f_{b,i}, \quad A(u) = \frac{u^2 + 2}{u\sqrt{u^2 + 4}}, \quad (3)$$

where F_i is the observed flux at each of n observatory/filter combinations, $f_{s,i}$ and $f_{b,i}$ are the source and background fluxes for each of these combinations, and $A(u)$ is the magnification as a function of u, the source-lens projected separation normalized to the angular Einstein radius θ_E. In the standard (i.e., nonparallax) model, the motions of the observer, source, and lens are all assumed to be rectilinear, so u is given simply by the Pythagorean theorem,

$$u(t) = \sqrt{\beta^2 + \tau^2}, \quad \tau = \frac{t - t_0}{t_E}, \quad \beta = u_0, \quad (4)$$

where t_0 is the time of closest approach, $u_0 = u(t_0)$ is the impact parameter, and t_E is the Einstein timescale. This procedure almost always converges, although for some events with very distorted light curves the fit is rather poor. The two exceptions to this are MACHO-99-BLG-1 and OGLE-2003-BLG-32, which have such distorted light curves that t_E had to be held at a fixed value to permit convergence.

To search for parallax solutions, we adopt the geocentric frame of Gould (2004), i.e., the Galilean frame that is coincident with the position and velocity of the Earth at the peak of the event. In this frame, the predicted fluxes are given by equations (3) and (4), but with β and τ adjusted by

$$\tau = \frac{t - t_0}{t_E} + \delta\tau, \quad \beta = u_0 + \delta\beta, \quad (5)$$

where

$$(\delta\tau, \ \delta\beta) = (\boldsymbol{\pi}_E \cdot \Delta s, \ \boldsymbol{\pi}_E \times \Delta s), \quad (6)$$

Δs is the positional offset of the Sun projected onto the sky (and normalized by an AU), and $\boldsymbol{\pi}_E$ is a new set of two parameters, the "vector microlens parallax."

3.1. Degeneracy Search

It is straightforward to find one parallax solution. We simply use the nonparallax solution (with $\boldsymbol{\pi}_E = 0$) as a seed and search for a minimum in χ^2. Since the parameters t_0, u_0, and t_E are very similar for the nonparallax solution and for the parallax solutions in the geocentric frame, this procedure always converges rapidly. However, it leaves open the question of whether there are other parallax solutions that are degenerate with this initial one. Smith et al. (2003) and Gould (2004) identified two types of degeneracy (the "constant-acceleration" and the "jerk-parallax" degeneracies, respectively) to which events are subject in the limit of weak parallax effects. In the geocentric frame, the constant-acceleration degeneracy is characterized by $u_0 \to -u_0$, with the

---

[6] An et al. (2002) have measured the path of a binary event, EROS BLG-2000-5. While they did not directly determine $\Delta\chi^2$, their error estimate for π_E is 3%, indicating a 30 σ detection, which would appear to meet our $\Delta\chi^2$ criterion. In addition, Kubas et al. (2005) measured the π_E for the binary event OGLE-2002-BLG-069 to a precision of 16% (after rescaling errors), corresponding to 6 σ, which probably would not meet our $\Delta\chi^2$ criterion. However, in any case, binary parallax events are much more complicated than point-lens events, so we exclude them from consideration here.

[7] Data available at http://www.macho.mcmaster.ca.

[8] Data available at http://www.massey.ac.nz/~iabond/alert/alert.html.

[9] Data available at http://ogle.astrouw.edu.pl/ogle3/ews/ews.html.

TABLE 1

MICROLENSING PARALLAX EVENTS

		CELESTIAL		ECLIPTIC		GALACTIC							
EVENT	REFERENCES	R.A.	Decl.	λ	β	l	b	m_{base}	POINTS	STANDARD $\Delta\chi^2$	BEST χ^2	D	XALLARAP $\Delta\chi^2$	RENORMALIZATION FACTOR
MB104C............	1	18 03 34.0	−28 00 19	270.790	−4.568	2.797	−2.933	16.4	870−23	1647.28	810.36	4	1.27	0.8/0.85, 0.8/0.92
MB96-5	1	18 05 02.5	−27 42 17	271.119	−4.270	3.219	−3.071	19.0	2284−5	2027.74	2262.85	2	12.85	1.323, 1.221, 0.947
MB96-12	1, 2	18 03 53.2	−27 57 36	270.861	−4.524	2.871	−2.973	16.9	2440−11	12397.19	2400.78	3	1.05	1.685, 0.786, 0.350, 1.006, 1.070
MB98-6	1	17 57 32.8	−28 42 45	268.762	−5.267	1.526	−2.132	18.5	2294−3	557.70	2274.88	2	15.84	1.212, 0.957, 0.556, 0.965
MB99-1	1	18 08 50.0	−30 31 56	271.917	−7.106	1.138	−5.162	18.0	793−5	1223.97	755.99	2	15.59	1.202, 0.933, 0.503, 0.864
MB99-8	1	17 56 25.2	−29 40 31	269.218	−6.237	0.569	−2.401	14.5	1085−4	56.51	1063.74	2	14.72	1.596, 1.299, 0.934, 1.591
MB179-A		18 08 58.4	−26 08 08	272.016	−2.712	5.019	−3.076	19.6	394−1	227.24	383.00	1	8.76	0.673, 0.793
MB98-1		18 04 54.5	−27 25 50	271.092	−3.996	3.445	−2.911	18.4	3119−18	248.49	3073.90	1	**112.11**	0.879, 1.052
MB95-27		18 08 18.0	−28 28 53	271.169	−5.047	2.568	−3.499	19.5	1728−10	190.79	1691.65	4	**17.38**	1.023, 1.377, 1.136, 1.207, 1.271
MB99-22	3	18 05 05.3	−28 34 44	271.122	−5.144	2.460	−3.506	18.8	1319−4	742.99	1295.99	2	3.29	1.060, 1.211, 0.876, 0.731, 1.550
KB00-11............	4	17 57 07.9	−29 09 59	269.371	−5.729	1.087	−2.281	14.1	1857−4	6336.14	1389.92	2	0.33	1.488
OB99-19............	5	17 51 10.8	−33 03 44	268.126	−9.637	−2.923	−3.147	16.1	324−3	10506.61	312.99	1	19.75	1.290
OC99-01............	6	11 07 26.7	−61 22 31	208.114	−58.066	−69.192	−0.976	17.9	547−0	112.21	539.98	2	5.13	1.323
OB00-43............	7	18 08 43.0	−32 24 40	271.863	−8.986	−0.533	−6.036	13.5	406−1	4307.26	397.00	1	6.13	1.679
OB33_4505	8	18 05 46.7	−28 25 32	271.275	−4.993	2.668	−3.563	19.3	185−0	213.05	169.83	2	**29.17**	1.131
OB02-100..........		18 06 47.9	−34 51 21	271.423	−11.425	−2.888	−6.849	17.9	112−1	139.38	103.00	2	**27.62**	1.352
OB02-334..........		18 00 20.3	−32 15 11	270.072	−8.814	−1.254	−4.411	16.2	172−0	612.91	165.01	1	5.98	1.475
OB02-61............		17 35 56.0	−27 16 02	264.641	−3.940	0.285	2.696	17.4	202−1	138.86	193.01	2	**11.66**	1.627
OB03-188..........		17 56 05.6	−33 02 46	269.169	−9.610	−2.389	−4.028	16.5	925−0	194.76	917.01	2	8.21	1.328, 0.951
OB03-32............		17 54 55.0	−31 00 40	268.901	−7.577	−0.751	−2.792	15.7	269−4	8042.35	244.26	2	12.84	1.421
OB03-84............		17 56 05.6	−33 02 46	269.169	−9.610	−2.389	−4.028	20.3	213−0	264.97	206.01	2	3.89	1.493
EB-29	2	18 10 56.2	−29 24 24	271.519	−5.977	1.930	−4.260	14.3	523−2	129.46	511.00	2	0.86	0.572, 0.724

NOTES.—OB99-32 was also monitored by MACHO as MACHO-99-BLG-22. The event names are abbreviated as follows: MByy-xx = MACHO-yy-BLG-xx, OByy-xx = OGLE-ccyy-BUL-xx, KByy-xx = MOA-ccyy-BUL-xx, OB33_4505 = sc33_4504, OC99-01 = OGLE-1999-CAR-01, EB-29 = EROS-BLG-29. This table lists all 22 events examined in this paper. The column m_{base} gives Johnson/Cousins R band for MACHO events and Cousins I band for all others. The column "D" gives the number of degenerate solutions ($\Delta\chi^2 < 10$). The degenerate solutions are in bold print in Table 2. The events with "Xallarap $\Delta\chi^2$" in bold are xallarap candidates.

REFERENCES.—(1) Bennett et al. 2002; (2) Afonso et al. 2003; (3) Mao et al. 2002; Bennett et al. 2002; Agol et al. 2002; (4) Bond et al. 2001; (5) Smith et al. 2002; (6) Mao 1999; (7) Soszyński et al. 2001; (8) Smith et al. 2002, 2003.

other parameters changing very little. The jerk-parallax degeneracy sends

$$\pi_{E,\parallel} \rightarrow \pi_{E,\parallel}, \quad \pi_{E,\perp} \rightarrow -(\pi_{E,\perp} + \pi_{j,\perp}), \qquad (7)$$

where the parallel and perpendicular directions are defined by the Sun's apparent acceleration at t_0 and π_j is the jerk parallax. In this case also, the remaining parameters change very little. Gould (2004) gives the exact formula for π_j, but in the approximation that the Earth's orbit is circular, the perpendicular component is

$$\pi_{j,\perp} = -\frac{4}{3}\frac{\mathrm{yr}}{2\pi t_E}\frac{\sin\beta_{\mathrm{ec}}}{(\cos^2\psi\sin^2\beta_{\mathrm{ec}} + \sin^2\psi)^{3/2}}, \qquad (8)$$

where β_{ec} is the ecliptic latitude of the event and ψ is the phase of the peak of the event relative to opposition.

3.2. Constant-Acceleration Degeneracy

The constant-acceleration degeneracy is the most common and easiest to identify, and we therefore look for it first. It is obtained by using the first parallax solution as a seed but with the sign of u_0 reversed. While this always converges to a new solution, in five cases the two solutions are not truly degenerate since one of these two has a significantly worse χ^2 or heavy negative blending. If this potential degeneracy is not realized, then the other possible degeneracies are not present either.

3.3. Jerk-Parallax Degeneracy

Since the Galactic bulge lies close to the ecliptic, the Sun's projected apparent acceleration is generally parallel to the ecliptic, which at the position of the Galactic bulge lies along the east-west axis. The vector-parallax components $\pi_{E,\parallel}$ and $\pi_{E,\perp}$ are therefore approximately aligned with $\pi_{E,E}$ and $\pi_{E,N}$, the east and north components of this vector. Moreover, from equation (8) one finds that near the ecliptic, $\pi_{j,\perp} \sim 0$. Hence, equation (7) becomes approximately

$$\pi_{E,E} \rightarrow \pi_{E,E}, \quad \pi_{E,N} \rightarrow -\pi_{E,N}. \qquad (9)$$

We therefore generally make this substitution in the original solution to obtain a seed to search for the jerk-parallax degenerate solution. When this fails, we use the more exact formula of Gould (2004). Three of the 22 events have at least three solutions.

When the search for a third solution is successful, we reverse the sign of u_0 in this solution to obtain a seed to search for a fourth solution. Only 2 of the 22 events have four distinct solutions.

3.4. Ecliptic Degeneracy

As noted by Jiang et al. (2004), events that lie exactly on the ecliptic suffer a twofold degeneracy. Unlike the degeneracies identified by Smith et al. (2003) and Gould (2004), which are perturbative (to fourth order in time) and so can be broken for events that are sufficiently long or have sufficiently high quality data, the ecliptic degeneracy is exact to all orders. Since the bulge lies near the ecliptic, one expects this degeneracy to apply approximately to bulge events. From simple geometric considerations, the exact ecliptic degeneracy takes

$$u_0 \rightarrow -u_0, \quad \pi_{E,\perp} \rightarrow -\pi_{E,\perp}. \qquad (10)$$

Hence, toward the bulge, a good seed for the approximate ecliptic degeneracy can be obtained by the substitutions $u_0 \rightarrow -u_0$,
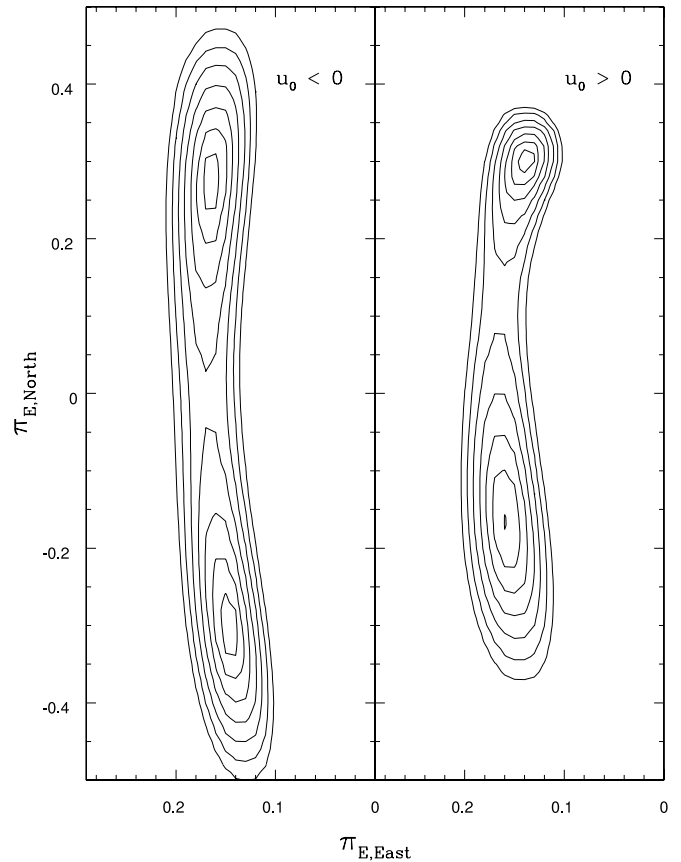

FIG. 1.—The $\Delta\chi^2$ contour map in the π_E plane for event MACHO-104-C. The pair of solutions in each panel is the jerk-parallax degeneracy. The solutions for positive u_0 and negative u_0 are at similar π_E because of the constant-acceleration degeneracy. The ecliptic degeneracy identifies the upper (lower) solution in the left panel with the lower (upper) solution in the right panel.

$\pi_{E,N} \rightarrow -\pi_{E,N}$. While we did not, in fact, locate this degeneracy in this manner, we find in retrospect that almost all of the events for which there are at least two solutions do in fact suffer from the ecliptic degeneracy and that it could have been found by the above substitution. What occurred in practice is that when we reversed the sign of u_0, but not $\pi_{E,N}$ (see § 3.2), the minimization procedure drove $\pi_{E,N}$ to the opposite sign anyway.

3.5. Solutions

Once all the parallax solutions are found for a given event, we focus our attention on the one with the lowest χ^2. We recursively remove outliers and rescale the errors so that χ^2 per degree of freedom (dof) is equal to unity. We terminate this procedure when the largest outlier has $\chi^2 < 14$. This cleaned and renormalized data set is used to evaluate all solutions. A χ^2 map in the π_E plane is generated for each solution to verify that all degenerate solutions have been identified. This is shown for event MACHO-104-C in Figure 1 and for event MACHO-179-A in Figure 2. Each solution is listed in Table 2. Again, most of the table headings are self-evident. The source magnitude is derived from the source flux for the band for which the baseline magnitude (derived from $f_s + f_b$) is given in Table 1. For MACHO events, this is actually a combination of the two observed bands. The column $\eta_b \equiv f_b/(f_s + f_b)$ gives the ratio of unlensed background light flux to the total baseline flux. The "geocentric" parameters are those obtained in the fit. The "heliocentric" parameters are derived from these and describe the event as it would be seen from the Sun. In particular, θ is the angle of the
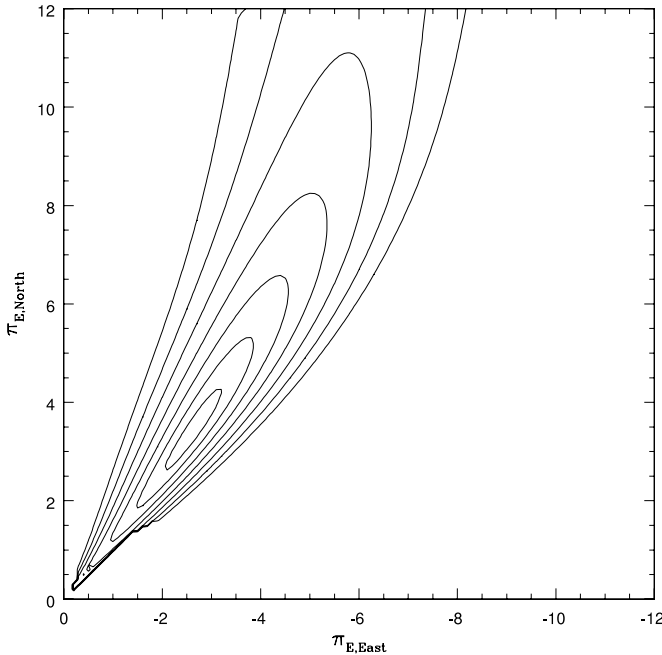
Fig. 2.—The $\Delta\chi^2$ contour map in the π_E plane for event MACHO-179-A.

lens-source relative motion, counterclockwise (celestial) north through east. An asterisk after the $\Delta\chi^2$ indicates that the solution has the background flux parameter ($f_{b,i}$ in eq. [3]) fixed to zero because the unconstrained solution (listed in the preceding row) has an unrealistically negative blend. (Blending can be slightly negative, while still remaining "physical," because the "sky" in crowded bulge fields comes partly from a mottled background of MS stars. If this background happens to be lower at the source position than at neighboring positions, f_b will be slightly negative. See Park et al. 2004 and Jiang et al. 2004.) The column "D" gives the number of degenerate solutions. Solutions in this paper are classified as "degenerate" if $\Delta\chi^2 < 10$ and the fit has realistic blending (unlike some of the parallax solutions of EROS-BLG-29). The degenerate solutions are in bold print in Table 2. We now comment on individual events.

Event MACHO-104-C, the first microlensing parallax event ever discovered (Alcock et al. 1995), is one of two events in our sample to have four degenerate parallax solutions. In this case all four solutions have $\Delta\chi^2 < 1$. This is surprising considering that the parallax fit is well constrained: the standard microlensing model has $\Delta\chi^2 = 1647$ relative to the best parallax solution. Bennett et al. (2002) found only one solution. Figure 1 shows $\Delta\chi^2$ contours (1, 4, 9, 16, 25, 36, 49) in the π_E plane.

Event MACHO-96-BLG-5 has been previously identified as a BH candidate (Bennett et al. 2002). We include the R_{MACHO} and B_{MACHO} bands along with follow-up R-band observations from the MACHO/GMAN Project (Becker 2000). We have excluded R_{MACHO} data from the 1999 season because the red CCD was changed and this could create a systematic offset. If we do include these additional data, the best-fit solution increases its geocentric timescale from 546 ± 165 to 698 ± 303 days and the $\tilde{r}_E$ increases from 16 ± 5 to 21 ± 9 AU. Additionally, the blending fraction increases slightly. This event is nearly at baseline and has no significant slope so including it as a separate band gives no leverage on further constraining the solution. The two degenerate solutions differ in velocity direction by $\sim100°$. This difference affects the mass estimate of the lens (see § 4.3). This event suffers from the ecliptic degeneracy.

Event MACHO-96-BLG-12 was initially found to have four degenerate solutions. After we rescaled the errors and removed 10 outliers, two of the solutions merged, leaving only three degenerate solutions. We include the R_{MACHO} and B_{MACHO} bands along with follow-up R-band observations from the MACHO/GMAN Project. After adding 1275 EROS data points in the R_{EROS} and B_{EROS} bands, we find that the previous best solution becomes the worst and the previous second best solution becomes the best. However, since the entire range of $\Delta\chi^2$ is only 3.25, such fluctuations are not unexpected. This event suffers from the ecliptic degeneracy.

Event MACHO-98-BLG-6 has also been previously identified as a BH candidate (Bennett et al. 2002; see § 4.3). We include the R_{MACHO} and B_{MACHO} bands along with follow-up R-band observations from the MACHO/GMAN and the Microlensing Planet Search (MPS) Project (Rhie et al. 1999). This event suffers from the ecliptic degeneracy.

Event MACHO-99-BLG-1 includes R_{MACHO} and B_{MACHO} bands along with follow-up R-band observations from the MACHO/GMAN and MPS Projects. This event suffers from the ecliptic degeneracy.

Event MACHO-99-BLG-8 includes R_{MACHO} and B_{MACHO} bands along with follow-up R-band observations from the MACHO/GMAN and MPS. This event suffers from the ecliptic degeneracy.

Event MACHO-179-A has only one solution, which has an unusually small $\tilde{r}_E = 0.23$. In § 4.5 we show that this small $\tilde{r}_E$ suggests that the lens is a brown dwarf. Figure 2 shows $\Delta\chi^2$ contours (1, 4, 9, 16, 25, 36, 49) in the π_E plane.

Event MACHO-95-BLG-27 includes follow-up R- and B-band observations from MACHO/GMAN and University of Toronto Southern Observatory (UTSO) R-band observations. We find that this event has four degenerate solutions. This relatively high magnification ($A_{max} \sim 40$) event shows no evidence for finite-source effects.

Event MACHO-99-BLG-22 was discovered by MACHO and then found by OGLE as OGLE-1999-BUL-32 independently 2 months later. We include data from both collaborations, as well as EROS B_{EROS} band, MACHO/GMAN, and MPS data. However, we exclude the MACHO R data because they are corrupted. Mao et al. (2002) searched for degeneracies but failed to find any. We find two highly degenerate solutions with $\Delta\chi^2 = 0.75$, another example of the ecliptic degeneracy. However, this newly discovered solution is very similar to the previous one and has a very small impact on the lens mass estimate in § 4.3.

Event MOA-2000-BLG-11 suffers from the ecliptic degeneracy.

Event OGLE-1999-BUL-19 has no degeneracies. Smith et al. (2002) also searched for degeneracies and also found none.

Event OGLE-1999-CAR-01 has two solutions after reduction by the OGLE-III pipeline. When we first analyzed this event, we had only the DoPhot photometry, which resulted in four degenerate solutions. This shows how improved reduction can break degeneracies. This is the only event we examined that is not near the ecliptic. Mao (1999) only identified one solution.

Event OGLE-2000-BUL-43 does not have any degenerate solutions. Soszyński et al. (2001) found two solutions with $\Delta\chi^2 = 6.8$. When using the same data set (which ends 3 days before the peak), we found the same two solutions with $\Delta\chi^2 = 7.15$. After including three seasons of data after the peak from OGLE-III, the degeneracy is broken. Our analysis is based on a rereduction of OGLE-II images using the OGLE-III image subtraction pipeline.

We find that sc33_4505 has two solutions with $\Delta\chi^2 = 8.23$. Smith et al. (2003) searched for degeneracies of this event and

TABLE 2
MICROLENSING PARALLAX SOLUTIONS

		GEOCENTRIC							HELIOCENTRIC			
EVENT	$\Delta\chi^2$	t_0 (JD)	u_0	t_E (days)	$\pi_{E,N}$	$\pi_{E,E}$	m_{source}	η_b	$\tilde{v}$ (km s^{-1})	θ	$\tilde{r}_E$ (AU)	t_E (days)
MB104C	1647.28	−882.60(5)	−0.073(1)	179(2)	. . .	. . .	16.76(2)	0.27	. . .	. . .	. . .	. . .
	0.37	−884.33(7)	−0.083(2)	169(3)	0.28(4)	0.163(6)	16.58(2)	0.15	47(4)	52.6(9)	3.1(3)	112(2)
	0.00	−884.28(6)	0.051(2)	232(9)	0.30(1)	0.138(5)	17.15(5)	0.50	38(1)	54.6(4)	3.0(1)	136(3)
	0.23	−884.27(6)	−0.085(1)	148(2)	−0.30(4)	0.147(6)	16.56(2)	0.13	47(4)	128.6(8)	3.0(3)	108(2)
	0.97	−884.33(7)	0.099(3)	139(3)	−0.17(3)	0.158(6)	16.38(4)	−0.03	70(6)	122.4(3.9)	4.4(4)	107(3)
MB96-5	2027.74	410.8(9)	−0.040(1)	666	. . .	. . .	21.11(2)	0.88	. . .	. . .	. . .	. . .
	1.15	414.8(10)	−0.048(11)	381(83)	0.042(10)	0.09(2)	20.84(27)	0.83	23(1)	37(2)	10(2)	744(159)
	0.00	417.1(1.1)	0.033(10)	546(165)	−0.023(7)	0.06(2)	21.19(36)	0.87	29(1)	135(3)	16(5)	967(291)
MB96-12	12397.19	391.22(3)	−0.0245(4)	247(4)	. . .	. . .	18.00(2)	0.65	. . .	. . .	. . .	. . .
	0.64	391.70(2)	−0.0618(11)	99(1)	−0.03(1)	0.257(6)	16.95(2)	0.08	47.2(10)	102(5)	3.86(11)	141(2)
	0.00	391.69(2)	0.0611(10)	100(1)	−0.03(1)	0.248(5)	16.96(2)	0.09	48.9(5)	101(4)	4.00(8)	141(2)
	3.26	391.70(2)	−0.0633(12)	96(2)	0.10(2)	0.269(9)	16.93(2)	0.05	42.9(1.7)	63(4)	3.50(16)	141(2)
MB98-6	557.70	1020.6(2)	−1.244(237)	67(9)	. . .	. . .	15.191(506)	−20.45	. . .	. . .	. . .	. . .
	925.83*	1022.4(2)	−0.229(1)	226(2)	. . .	. . .	18.508(3)	0.00	. . .	. . .	. . .	. . .
	0.00	1028.0(5)	−0.199(21)	307(25)	−0.08(2)	0.089(8)	18.672(154)	0.15	66(5)	119(7)	8.5(9)	220(15)
	7.00	1028.4(4)	0.177(24)	301(32)	0.01(2)	0.091(5)	18.800(187)	0.24	84(4)	86(9)	10.9(7)	225(19)
MB99-1	1223.97	1344.1(3)	0.317(3)	218	. . .	. . .	17.89(1)	−0.11	. . .	. . .	. . .	. . .
	0.37	1351.5(1.4)	−0.259(63)	405(99)	−0.31(4)	0.22(4)	18.24(34)	0.21	36(1)	103(2)	2.6(3)	124(19)
	0.00	1351.6(9)	0.295(70)	291(62)	0.22(2)	0.24(3)	18.06(34)	0.07	44(2)	73(1)	3.1(3)	120(18)
MB99-8	56.51	1357.3(1)	−0.8978(640)	63.6(3.0)	. . .	. . .	12.325(153)	−6.40	. . .	. . .	. . .	. . .
	1190.26*	1356.8(1)	−0.2345(8)	152.6(5)	. . .	. . .	14.507(1)	0.00	. . .	. . .	. . .	. . .
	0.00	1358.9(4)	−0.1718(780)	249.3(102.4)	0.09(8)	0.235(25)	14.971(582)	0.35	55(13)	80(7)	4.0(2)	124(27)
	0.57	1358.9(3)	0.1930(739)	212.9(72.6)	−0.03(3)	0.227(9)	14.821(500)	0.26	64(13)	95(3)	4.4(2)	117(22)
MB179-A	227.24	247.1(3)	0.139(44)	132(35)	. . .	. . .	20.252(383)	0.48	. . .	. . .	. . .	. . .
	20.75	250.4(2)	−0.870(196)	22(4)	−10.1(1.7)	−9.5(1.2)	17.362(475)	−6.45	25.6(2)	97.7(7)	0.07(1)	4.9(7)
	64.66*	249.9(2)	−0.228(4)	60(2)	−4.0(2)	−4.5(4)	19.561(9)	0.00	25.8(1)	95.7(5)	0.17(1)	11.2(8)
	0.00	250.8(3)	0.163(50)	83(21)	3.4(8)	−2.6(6)	19.968(382)	0.32	26.6(1)	80.4(6)	0.23(5)	15.2(3.4)
MB98-1	248.49	889.6(2)	−0.089(6)	128(8)	. . .	. . .	18.68(8)	0.25	. . .	. . .	. . .	. . .
	59.70	886.3(3)	−0.044(3)	262(19)	0.27(2)	0.33(3)	19.57(9)	0.66	14.1(6)	33(2)	2.3(2)	283(20)
	99.45	886.4(2)	0.032(3)	285(28)	0.25(2)	0.18(2)	19.92(12)	0.75	19.3(10)	22(1)	3.2(3)	287(28)
	77.38	886.1(2)	−0.039(3)	230(17)	−0.32(2)	0.26(2)	19.69(9)	0.69	14.0(6)	148(2)	2.4(2)	295(22)
	0.00	886.4(3)	0.070(5)	170(11)	−0.40(2)	0.51(4)	19.04(8)	0.43	11.3(4)	132(2)	1.5(1)	237(14)
MB95-27	190.79	−54.67(4)	−0.029(4)	263(36)	. . .	. . .	21.6(2)	0.85	. . .	. . .	. . .	. . .
	1.19	−55.05(6)	−0.025(5)	331(70)	−0.20(3)	−0.11(2)	21.7(2)	0.87	22.9(1.6)	162(6)	4.4(7)	329(58)
	0.00	−55.05(5)	0.023(5)	327(74)	−0.19(3)	−0.07(2)	21.8(3)	0.89	27.6(1.9)	163(6)	5.0(9)	314(61)
	3.81	−55.05(5)	−0.028(5)	267(48)	0.24(4)	−0.13(2)	21.6(2)	0.86	20.2(1.2)	18(6)	3.7(5)	314(50)
	7.45	−55.06(6)	0.029(5)	286(51)	0.25(4)	−0.17(3)	21.5(2)	0.85	16.0(9)	24(7)	3.3(5)	357(54)
MB99-22	742.99	1365.79(6)	−0.0357(2)	425	. . .	. . .	19.761(2)	0.63	. . .	. . .	. . .	. . .
	0.00	1365.31(7)	−0.0358(30)	419(33)	−0.010(9)	−0.039(5)	19.744(58)	0.59	74(9)	70(17)	24(4)	571(39)
	1.52	1365.34(7)	0.0359(35)	421(39)	0.001(5)	−0.038(5)	19.745(68)	0.59	80(5)	92(10)	26(4)	570(44)
KB00-11	6336.14	1799.48(2)	−0.133(2)	50.5(4)	. . .	. . .	14.358(9)	0.23	. . .	. . .	. . .	. . .
	0.45	1798.79(3)	−0.086(1)	70.2(7)	0.13(9)	−0.469(7)	14.877(8)	0.52	45.9(2.3)	102(12)	2.06(9)	77.5(8)
	0.00	1798.79(3)	0.086(1)	70.6(6)	0.07(4)	−0.471(6)	14.867(10)	0.52	47.0(8)	95(5)	2.10(4)	77.4(7)
OB99-19	10506.61	1628.15(6)	−0.107(1)	168(2)	. . .	. . .	16.230(9)	0.16	. . .	. . .	. . .	. . .
	539.52	1629.56(51)	−0.018(1)	2535(165)	0.113(7)	−0.003(1)	18.253(45)	0.85	11.5(1)	17.6(5)	8.84(55)	1331(83)
	0.00	1628.81(13)	0.096(1)	279(3)	−0.365(4)	−0.025(2)	16.362(11)	0.20	12.2(1)	168.2(5)	2.73(3)	387(5)

TABLE 2—*Continued*

		GEOCENTRIC							HELIOCENTRIC			
EVENT	$\Delta\chi^2$	t_0 (JD)	u_0	t_E (days)	$\pi_{E,N}$	$\pi_{E,E}$	m_{source}	η_b	$\tilde{v}$ (km s⁻¹)	θ	$\tilde{r}_E$ (AU)	t_E (days)
OC99-01..............	112.21	1284.0(1)	−0.22(1)	123(6)	...	...	18.60(5)	0.45	...	...	...	...
	0.00	**1282.7(2)**	**−0.25(4)**	**110(16)**	**−0.07(3)**	**−0.08(4)**	**18.42(13)**	**0.35**	**142.8(14.2)**	**38.3(26.3)**	**9.1(1.3)**	**110(7)**
	1.57	**1282.7(2)**	**0.24(4)**	**113(13)**	**−0.06(2)**	**−0.04(3)**	**18.48(13)**	**0.38**	**214.2(22.0)**	**28.1(28.6)**	**13.7(1.5)**	**110(6)**
	30.96	1282.5(1)	−0.22(4)	89(13)	0.67(7)	−0.82(9)	18.62(15)	0.46	11.7(7)	140.5(7)	0.9(1)	139(9)
	10.44	1282.8(5)	0.19(3)	218(39)	0.36(4)	−0.51(5)	18.80(15)	0.54	17.3(1.0)	140.0(8)	1.6(2)	160(9)
OB00-43..............	4307.26	1874.1(3)	−0.0386(6)	383(5)	...	...	15.16(1)	0.79	...	...	...	...
	0.00	**1871.9(4)**	**−0.1317(53)**	**111(3)**	**−0.111(4)**	**0.228(9)**	**13.78(4)**	**0.26**	**40.2(8)**	**136.5(10)**	**3.94(15)**	**169(4)**
	83.10	1871.6(4)	0.0966(34)	143(4)	−0.074(3)	0.132(5)	14.15(3)	0.47	59.2(1.1)	134.3(1.5)	6.59(22)	192(5)
	100.61	1873.9(5)	−0.1803(77)	84(3)	0.248(8)	0.347(14)	13.32(4)	−0.13	28.2(5)	25.4(5)	2.35(9)	143(4)
OB33_4505..........	213.05	647.2(3)	−0.41(3)	165(9)	...	...	19.76(7)	0.36	...	...	...	...
	8.23	**641.2(4)**	**−0.50(8)**	**125(14)**	**0.23(2)**	**−0.099(13)**	**19.45(16)**	**0.15**	**50(5)**	**6(4)**	**4.0(3)**	**136(13)**
	0.00	**640.7(5)**	**0.29(5)**	**203(29)**	**−0.15(1)**	**−0.027(9)**	**20.30(16)**	**0.61**	**57(5)**	**161(5)**	**6.4(5)**	**193(21)**
OB02-100.............	139.38	2448.12(2)	−0.042(2)	57(3)	...	...	18.81(4)	0.58	...	...	...	...
	0.68	**2448.19(2)**	**−0.029(4)**	**81(10)**	**2.1(3)**	**0.9(3)**	**19.23(9)**	**0.71**	**34.2(8)**	**74(3)**	**0.44(4)**	**22(2)**
	0.00	**2448.19(2)**	**0.028(4)**	**82(10)**	**1.8(2)**	**1.0(3)**	**19.25(9)**	**0.72**	**35.5(8)**	**75(3)**	**0.48(4)**	**23(2)**
OB02-334.............	612.91	2699.8(9)	−0.11(1)	260(19)	...	...	18.0179(765)	0.81	...	...	...	...
	7.84	2666.2(1.4)	−0.75(13)	41(5)	−0.52(8)	0.59(8)	14.3425(2416)	−4.47	36(3)	150(2)	1.3(2)	60(7)
	31.39*	2677.0(8)	−0.30(1)	81(1)	−0.23(3)	0.24(2)	16.1914(8)	0.00	48(6)	148(4)	3.0(4)	108(1)
	0.00	**2673.5(2.3)**	**0.19(4)**	**98(11)**	**0.17(2)**	**0.19(3)**	**16.4882(1690)**	**0.24**	**56(6)**	**31(4)**	**3.9(5)**	**118(12)**
OB02-61..............	138.86	2508.1(2)	−0.161(8)	200(8)	...	...	17.72(4)	0.28	...	...	...	...
	2.33	**2509.7(2)**	**−0.147(22)**	**191(17)**	**0.11(7)**	**0.062(7)**	**17.82(12)**	**0.35**	**75(42)**	**37(11)**	**7(4)**	**180(16)**
	0.00	**2509.8(2)**	**0.114(20)**	**235(31)**	**−0.12(3)**	**0.052(7)**	**18.13(13)**	**0.51**	**64(17)**	**147(4)**	**7(1)**	**208(24)**
OB03-188.............	194.76	2922.9(6)	−0.17(2)	158(11)	...	...	18.69(8)	0.87	...	...	...	...
	7.58	**2923.7(5)**	**−0.19(3)**	**126(17)**	**−0.18(4)**	**0.22(4)**	**18.51(13)**	**0.85**	**45(9)**	**141(7)**	**3.6(6)**	**137(17)**
	0.00	**2923.5(4)**	**0.15(3)**	**136(20)**	**−0.16(3)**	**0.14(2)**	**18.83(15)**	**0.89**	**57(10)**	**150(8)**	**4.7(7)**	**141(18)**
	12.10	2923.6(4)	−0.22(3)	99(10)	0.25(6)	0.20(3)	18.34(12)	0.82	44(11)	32(7)	3.1(6)	121(13)
OB03-32..............	8042.35	2909.4(3)	−1.020(7)	89	...	...	14.622(9)	−1.81	...	...	...	...
	0.00	**2927.4(2)**	**−0.467(31)**	**89(4)**	**0.234(12)**	**0.31(1)**	**16.073(67)**	**0.27**	**37(2)**	**45(2)**	**2.58(9)**	**117(5)**
	9.75	**2927.1(3)**	**0.383(30)**	**112(6)**	**−0.127(6)**	**0.24(1)**	**16.385(75)**	**0.45**	**47(1)**	**128(2)**	**3.68(13)**	**132(7)**
OB03-84..............	264.97	2757.9(3)	−0.219(35)	56(6)	...	...	18.98(13)	−1.55	...	...	...	...
	298.27*	2758.2(3)	−0.092(2)	103(3)	...	...	20.02(1)	0.00	...	...	...	...
	7.85	**2760.1(3)**	**−0.062(19)**	**149(39)**	**0.13(4)**	**−0.55(14)**	**20.46(21)**	**0.22**	**8.4(6)**	**177(6)**	**1.76(44)**	**361(92)**
	12.35	2760.2(2)	0.058(18)	150(40)	0.12(3)	−0.53(14)	20.51(21)	0.26	8.5(8)	172(4)	1.85(47)	375(98)
	0.00	**2760.0(2)**	**−0.069(20)**	**135(36)**	**−0.31(8)**	**−0.57(15)**	**20.35(21)**	**0.06**	**6.2(3)**	**159(5)**	**1.54(39)**	**430(109)**
	73.09	2759.3(3)	0.099(23)	112(22)	−0.42(8)	−0.66(12)	19.92(17)	−0.32	7.5(4)	156(5)	1.28(24)	297(56)
	75.43*	2759.3(3)	0.072(3)	147(9)	−0.32(2)	−0.51(3)	20.29(3)	0.00	7.6(4)	156(5)	1.66(10)	381(33)
EB-29	41.44	1253.4(3)	−0.394(19)	94.0(2.4)	...	...	13.7065(444)	−0.66	...	...	...	...
	129.46*	1254.5(2)	−0.263(1)	116.5(5)	...	...	14.2599(6)	0.00	...	...	...	...
	0.65	1252.1(5)	−0.426(25)	102.7(4.8)	0.23(4)	0.044(9)	13.5868(559)	−0.86	73(15)	7.2(1.7)	4.24(75)	99.3(4.1)
	83.97*	1253.6(4)	−0.263(1)	141.8(3.7)	0.26(2)	0.044(7)	14.2614(6)	0.00	48(5)	4.1(10)	3.73(29)	134.3(2.7)
	2.87	**1252.3(3)**	**0.185(16)**	**147.7(9.3)**	**0.27(1)**	**0.021(4)**	**14.7621(698)**	**0.37**	**46(4)**	**179.3(8)**	**3.73(17)**	**138.5(7.9)**
	0.00	**1252.3(3)**	**−0.280(19)**	**105.2(4.3)**	**−0.32(2)**	**0.042(5)**	**14.2068(588)**	**−0.05**	**47(5)**	**176.9(8)**	**3.06(24)**	**112.8(5.3)**
	1.24	1252.2(4)	0.529(43)	84.5(2.8)	−0.19(4)	0.050(10)	13.2339(847)	−1.57	100(23)	167.1(2.3)	5.11(1.17)	87.8(2.8)
	14.43*	1252.4(3)	0.270(1)	113.8(5)	0.19(2)	0.015(4)	14.2581(6)	0.00	81(6)	1.6(1.2)	5.17(41)	109.8(6)

NOTES.—Solutions in bold are degenerate ($\Delta\chi^2 < 10$). The column $\eta_b \equiv f_b/(f_s + f_b)$ gives the function of unlensed background light flux to the total baseline flux. The "geocentric" parameters are those obtained in the fit. The "heliocentric" parameters are derived from these and describe the event as it would be seen from the Sun. In particular, θ is the angle of the lens-source relative motion, counterclockwise (celestial) north through east. An asterisk after the $\Delta\chi^2$ indicates that the solution has the background flux parameter ($f_{b,i}$ in eq. [3]) fixed to zero because the unconstrained solution (listed in the preceding row) has an unrealistically negative blend.
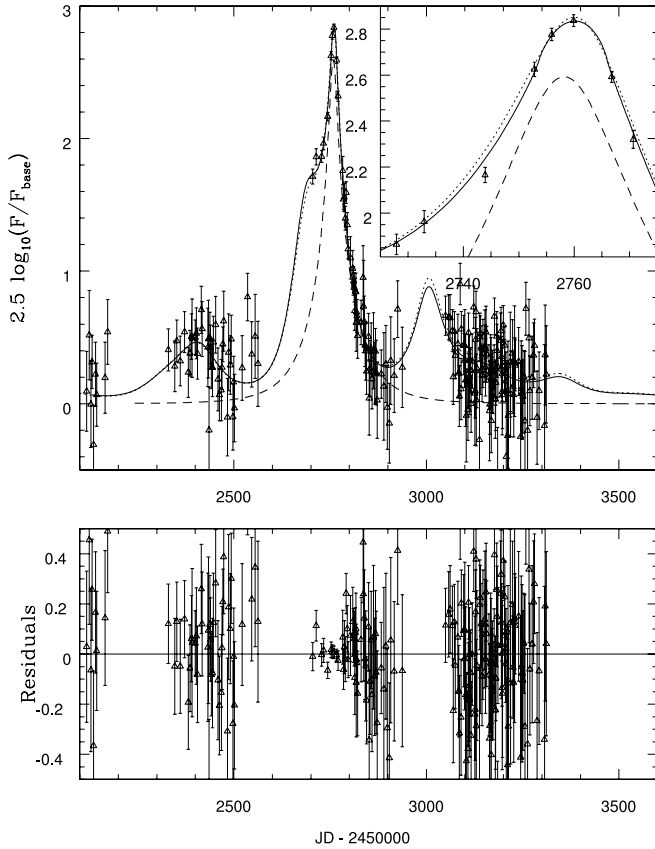
FIG. 3.—Light curve of OGLE-2003-BLG-84 planetary candidate. The solid line is the best parallax model with finite-source effects. The dotted line is the best parallax model *without* finite-source effects. The dashed line is the point-source nonparallax model. The inset in the top panel is an enlarged view of the light-curve peak. The bottom panel shows the residuals of the parallax model with finite-source effects.

found a second solution with $\Delta\chi^2 = 10.5$. The difference in $\Delta\chi^2$ derives from the fact that we rescaled our errors. This is another example of the ecliptic degeneracy.

Event OGLE-2002-BLG-100 is one of two events that have at least two solutions but do *not* suffer from the ecliptic degeneracy. This is not surprising since it is the farthest from the ecliptic of all the events toward the bulge.

Event OGLE-2002-BLG-334 has only one viable solution. The other potential solution is ruled out by severe negative blending.

Event OGLE-2002-BLG-61 suffers from the ecliptic degeneracy.

Event OGLE-2003-BLG-188 was also monitored as MOA-2003-BLG-61. We include these data in our analysis. It is one of two events with two or more solutions that do *not* suffer from the ecliptic degeneracy.

Event OGLE-2003-BLG-32 suffers from the ecliptic degeneracy.

Event OGLE-2003-BLG-84 is listed as a binary lens in Jaroszyński et al. (2004). We include the 2004 data in our analysis and find a hump in this previously unanalyzed year that is well modeled by the parallax solution. Moreover, as we discuss in § 5, the xallarap fit reproduces the Earth's orbital parameters, which would be most extraordinary if this were a binary event that just happened to be fitted by parallax. We infer that its complex structure (see Fig. 3) is indeed due to parallax. This event has two "ecliptic" degenerate solutions ($\Delta\chi^2 \leq 7.85$). Curiously one of these solutions predicts a large spike in the light curve between the 2003 and 2004 observing season, although the better

one does not. As we discuss in § 4.4, OGLE-2003-BLG-84 is a free-floating planet candidate.

Event EROS-BLG-29 suffers from the ecliptic degeneracy.

4. LIKELIHOOD MASS ANALYSIS

Even with a precise measurement of π_E, one cannot generally determine the lens mass M unless θ_E is also measured (see eqs. [1] and [2]). With the possible exception of OGLE-2003-BLG-84, none of the events analyzed in this paper have θ_E measurements.

Instead, we can estimate the likelihood of the lens mass using a prior MF together with prior probability distributions for the positions and velocities of the source and lens. Our model of the Milky Way consists of a double exponential disk with a Han & Gould (1996, 2003) barred bulge. We adopt $R_\odot = 8$ kpc for the Galactocentric distance of the Sun. Our disk has a scale length of 3500 pc and a scale height of 325 pc. We adopt a solar velocity $v_\odot = (10, 225, 7)$ km s^{-1} in the Galactocentric, rotation, and north polar directions and disk velocity dispersions of (40, 30, 20) km s^{-1} in these directions. We assume a mean disk rotation of 214 km s^{-1} (220 km s^{-1} rotation, less 6 km s^{-1} asymmetric drift). The bulge stars are assumed to have zero mean velocity with dispersion of 80 km s^{-1} in each direction. By itself, this would not be a self-consistent model of the Galaxy. Note that

$$G\Sigma h = k\sigma^2, \qquad (11)$$

where Σ is the surface density of the disk, h is the scale height, σ is the velocity dispersion, and k is a constant of order unity. Therefore, h and σ cannot be constants. We adjust these by making

$$\sigma \propto \Sigma^{1/3}, \quad h \propto \Sigma^{-1/3}. \qquad (12)$$

Since the bar most likely formed from a disk instability, there should be a paucity of disk stars in the bar region. Therefore, we removed the inner disk from our model within 2 kpc of the Galactic center. We find that this has little effect on the likelihood calculations. Furthermore, we include radial velocity measurements (Cavallo et al. 2003) to constrain the source position on events MACHO-98-BLG-6, MACHO-99-BLG-1, MACHO-99-BLG-8, and MACHO-99-BLG-22.

The Sgr dwarf galaxy can contribute to microlensing events (Cseresnjes & Alard 2001) and is included as a possible source. It is at a distance of 26.3 kpc (Monaco et al. 2004), and its stars are assumed to be moving 2.2 mas yr^{-1} toward Galactic north (Ibata et al. 1997) with negligible dispersion. Sgr dwarf RR Lyrae stars are ~2.6% as numerous as bulge RR Lyrae stars in the MACHO fields (Alcock et al. 1997a). This factor is included in our model.

We model Γ_{prior}, the expected microlensing rate prior to making an observation,

$$\frac{d^5\Gamma_{prior}}{dM\,dx_l\,dx_s\,d^2\mu_{rel}} = \rho_l(x_l)x_l^2 2\theta_E(M,\,x_l,\,x_s)\mu_{rel}\phi(M)$$

$$\times \rho_s(x_s)x_s^2 f(\mu_{rel};\,x_l,\,x_s)\left(\frac{x_s}{R_0}\right)^{-\beta}, \quad (13)$$

where x_l and x_s are the distances to the lens and source, respectively, $\rho_l(x_l)$ and $\rho_s(x_s)$ are the number density of each, $f(\mu_{rel};\,x_l,\,x_s)$ is the distribution of relative proper motions, μ_{rel}, given the source and lens positions, and $\phi(M) = dN/dM$ is the MF of lenses with

normalization $\int \phi(M)\, dM = 1$. Equation (13) is simply a rate derived from

$$\Gamma = n\sigma v_T, \quad n = \rho_l(x_l)\, dx_l\, \phi(M)\, dM,$$
$$\sigma = 2\theta_E x_l, \quad v_T = \mu_{\mathrm{rel}} x_l, \qquad (14)$$

where n is the number density, σ is the cross section, and v_T is the lens-source transverse velocity. The additional factors $f(\boldsymbol{\mu}_{\mathrm{rel}},\, x_l,\, x_s)\, d^2\boldsymbol{\mu}_{\mathrm{rel}}$ and $\rho_s(x_s) x_s^2 (x_s/R_0)^{-\beta}\, dx_s$ account for the distributions of lens-source relative proper motions and source distances. Here β is a parameter that characterizes the selection effects from more distant, fainter source stars. We use $\beta = 1$ for our calculations but find that changing it has little effect on the results.

The result of the observations is to measure $\tilde{v}$ and $\tilde{r}_E$, which yields a trivariate error distribution function $G(\tilde{r}_E - \tilde{r}_{E,\mathrm{obs}},\, \tilde{\boldsymbol{v}} - \tilde{\boldsymbol{v}}_{\mathrm{obs}})$ relative to the best-fit values $\tilde{r}_{E,\mathrm{obs}}$ and $\tilde{\boldsymbol{v}}_{\mathrm{obs}}$. The product of this function with equation (13) gives the posterior rate Γ_{post}, which we integrate over all variables except M,

$$\frac{d\Gamma_{\mathrm{post}}}{dM} = \int \frac{d^5\Gamma_{\mathrm{prior}}}{dM\, dx_l\, dx_s\, d^2\boldsymbol{\mu}_{\mathrm{rel}}}$$
$$\times G(\tilde{r}_E - \tilde{r}_{E,\mathrm{obs}},\, \tilde{\boldsymbol{v}} - \tilde{\boldsymbol{v}}_{\mathrm{obs}})\, dx_l\, dx_s\, d^2\boldsymbol{\mu}_{\mathrm{rel}}. \qquad (15)$$

Before performing the integration, we must switch integration variables $\boldsymbol{\mu}_{\mathrm{rel}} \to \tilde{\boldsymbol{v}}$ and $x_l \to \tilde{r}_E$. We multiply by the Jacobian,

$$\frac{dx_l}{d\tilde{r}_E}\frac{d^2\boldsymbol{\mu}_{\mathrm{rel}}}{d^2\tilde{\boldsymbol{v}}} = \frac{2x_l^2 \pi_{\mathrm{rel}}}{\mathrm{AU}\,\tilde{r}_E}\left(\frac{\pi_{\mathrm{rel}}}{\mathrm{AU}}\right)^2, \qquad (16)$$

which yields

$$\frac{d\Gamma_{\mathrm{post}}}{dM} = 4\phi(M)\int dx_s\, d\tilde{r}_E\, d^2\boldsymbol{v}\, \rho_l(x_l) x_l^4 \left(\frac{\pi_{\mathrm{rel}}}{\mathrm{AU}}\right)^5 \tilde{v}\rho_s(x_s) x_s^2$$
$$\times \left(\frac{x_s}{R_0}\right)^{-\beta} f(\boldsymbol{\mu}_{\mathrm{rel}};\, x_l,\, x_s) G(\tilde{r}_E - \tilde{r}_{E,\mathrm{obs}},\, \tilde{\boldsymbol{v}} - \tilde{\boldsymbol{v}}_{\mathrm{obs}}), \quad (17)$$

where $\pi_{\mathrm{rel}}/\mathrm{AU} = (x_l^{-1} - x_s^{-1})$, $\boldsymbol{\mu}_{\mathrm{rel}} = \tilde{\boldsymbol{v}}\pi_{\mathrm{rel}}/\mathrm{AU}$, and x_l itself are implicit functions of $\tilde{r}_E = (\kappa M/\pi_{\mathrm{rel}})^{1/2}$, $\tilde{\boldsymbol{v}}$, and x_s. Finally, we assume that over the range that G is substantially different from zero, the remainder of the integrand varies relatively little. It is then appropriate to replace G by a three-dimensional δ-function. Integration of equation (17) then yields

$$\frac{d\Gamma_{\mathrm{post}}}{dM} = 4\phi(M)\int dx_s\, \rho_l(x_l) x_l^4 \left(\frac{\pi_{\mathrm{rel}}}{\mathrm{AU}}\right)^5 \tilde{v}_{\mathrm{obs}}\rho_s(x_s) x_s^2$$
$$\times \left(\frac{x_s}{R_0}\right)^{-\beta} f(\tilde{\boldsymbol{v}}_{\mathrm{obs}}\pi_{\mathrm{rel}}/\mathrm{AU};\, x_l,\, x_s), \qquad (18)$$

where again x_l and π_{rel} are implicit functions of $\tilde{r}_E$, x_s, and M.

4.1. Mass Function

The MF of the bulge MS has been measured in both the optical (Holtzman et al. 1998) and the infrared (Zoccali et al. 2000) using *Hubble Space Telescope* (*HST*) observations. For purposes of this paper, we adopt an MS MF that is consistent with those measurements (but without corrections for binaries),

$$\frac{dN}{dM} = k\left(\frac{M}{M_{\mathrm{brk}}}\right)^{\alpha}, \quad M_{\mathrm{brk}} = 0.7\, M_\odot, \qquad (19)$$

where k is a constant and

$$\alpha = \begin{cases} -1.3, & 0.03\, M_\odot < M < M_{\mathrm{brk}}, \\ -2.0, & M_{\mathrm{brk}} < M \lesssim 1\, M_\odot. \end{cases} \qquad (20)$$

The upper of limit of $\sim 1\, M_\odot$ is the approximate position of the turnoff. The lower limit is arbitrary and simply extends the slope of the Zoccali et al. (2000) observations from their last measured point at $0.15\, M_\odot$ into the brown dwarf regime. The MF may well extend even further, but events showing significant parallax distortion are typically too long to be caused by lower mass lenses.

We assume that all MS stars in the range $1\, M_\odot < M < 8\, M_\odot$ have now become WDs and that the total number can be found by extending the upper MS power law $\alpha = -2.0$ through this higher mass regime. That is, $N_{\mathrm{WD}} = \frac{7}{8}k M_{\mathrm{brk}}^2/M_\odot$. Of course, there is no evidence whatever that the slope does continue in this regime. A more popular slope is the Salpeter value $\alpha = -2.35$. Had we chosen this steeper slope, the estimate for N_{WD} would be reduced by a factor of 0.80. For the distribution of WD masses, we adopt the MF shown in Figure 11c of Bragaglia et al. (1995) based on observations of 164 hot WDs. We assume that all MS stars $8\, M_\odot < M < 40\, M_\odot$ become NSs, with masses that are centered at $M = 1.35\, M_\odot$ and with Gaussian dispersion of $0.04\, M_\odot$ (Thorsett & Chakrabarty 1999). We assume that all MS stars $40\, M_\odot < M < 100\, M_\odot$ become BHs, with masses that are centered at $M = 7\, M_\odot$ and with Gaussian dispersion of $1\, M_\odot$. We also assume that the power law $\alpha = -2$ extends throughout this entire regime.

The lens contributes to the baseline light of an event (Kamionkowski 1995; Buchalter & Kamionkowski 1997; Nemiroff 1997; Han 1998). Thus, the blending of the event gives an upper limit on the brightness of a lens. This brightness limit provides an upper limit on the mass of an MS lens. We model extinction as a double exponential with a dust scale length of 3500 pc and a scale height of 130 pc with a local extinction of 0.4 mag kpc^{-1}. At each source and lens distance we use the Cox (2000) mass-luminosity relationship to cut off the MS portion of the MF.

4.2. Likelihood Results

The relative Γ likelihoods for each type of lens are shown in Figures 4, 5, and 6, where they are normalized to unity and so expressed as a probability distribution function. The dotted line is the expected distribution of each event from our Galactic model.

Figure 7 shows a composite of the expected microlensing rate based on our Galactic model for the non-(BH/BD/xallarap) events. This figure shows how the events in this paper are not typical but instead have lenses that are relatively more massive and closer to us. Also, Table 3 shows the contribution of the various lens and source populations to the total likelihood. "Both" refers to both disk and bulge lenses, and "All" refers to disk, bulge, and Sgr sources. When there is more than one solution, we evaluate each solution separately and then combine them using Bayes's theorem, $P(M|D) = P(M)P(D|M)/P(D) = P(M)\exp(-\chi^2/2)$, where $P(M|D)$ is the probability of the model given the data, $P(M)$ is the prior probability of the model, $P(D|M) = \exp(-\chi^2/2)$ is the probability of the data given the model, and $P(D)$ is a normalization factor, which is unimportant for our relative likelihood comparisons. Thus, we weight the output of equation (18) by $\exp(-\Delta\chi^2/2)$ and add the results together to obtain a total likelihood for each event. The displayed numbers for each solution are presented such that the totals for each
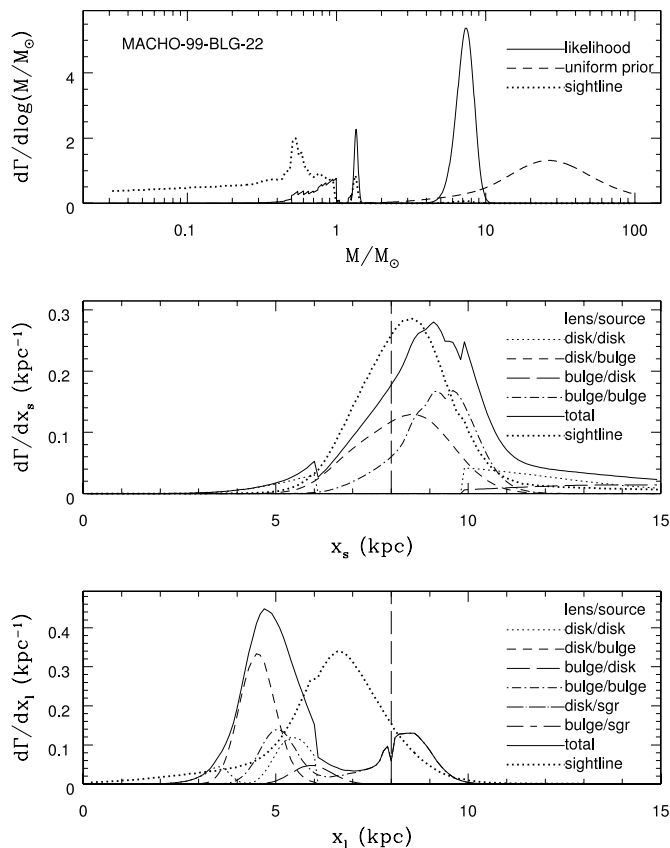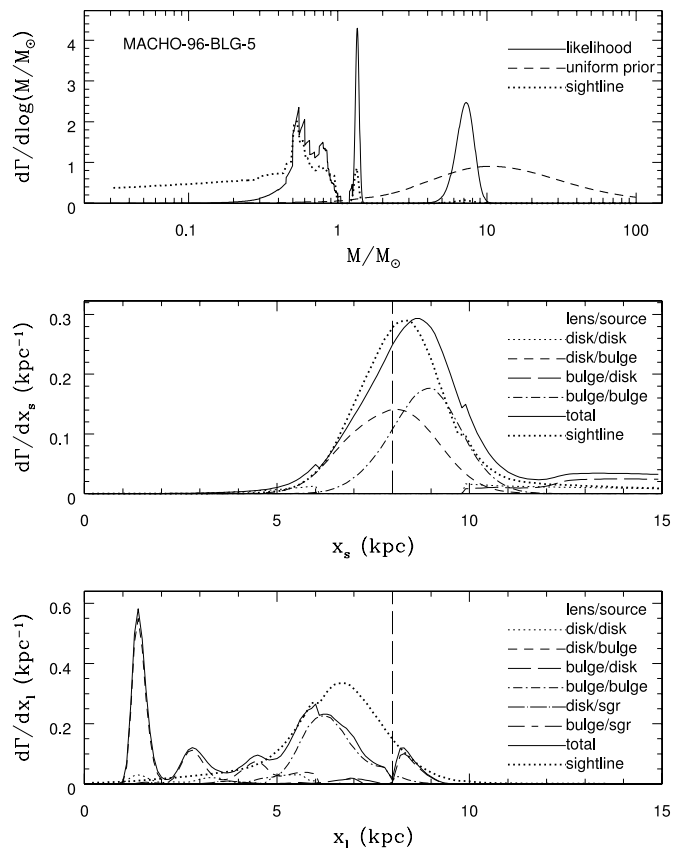
FIG. 4.—Relative likelihoods vs. mass, lens distance, and source distance for MACHO-99-BLG-22. In the top panel, the solid line is the result of our likelihood mass calculations. The dotted line is the expected distribution along this sight line from our Galactic model. The dashed line is the mass likelihood with a uniform prior in logarithmic mass. The middle and bottom panels give the likelihood of the source and lens distances, respectively.

FIG. 5.—Relative likelihoods vs. mass, lens distance, and source distance for MACHO-96-BLG-5. In the top panel, the solid line is the result of our likelihood mass calculations. The dotted line is the expected distribution along this sight line from our model. The dashed line is the mass likelihood with a uniform prior in logarithmic mass. The middle and bottom panels give the likelihood of the source and lens distances, respectively.

solution all add to make up the combined table. The weight factor is listed next to the solution number.

4.3. Black Hole Candidates

Three parallax events have been identified in the literature as BH candidates, MACHO-96-BLG-5, MACHO-98-BLG-6, and MACHO-99-BLG-22. We assess these candidates by evaluating the relative probability that they lie in one of four stellar classes: MS stars and brown dwarfs, WDs, NSs, and BHs. For each solution we place an upper limit on the mass of an MS lens based on blending of the light curve. There are additional photometric constraints available for MACHO-96-BLG-5.

Bennett et al. (2002) obtained *HST* images of MACHO-96-BLG-5 to constrain the blending of the source star. They found that 31% of the total flux was from the source star or from other stars (such as the lens) that are very closely aligned with it. However, as they note, this does not rule out that another blended star (possibly the lens) is unresolved by *HST*. The best-fit parallax solution yields a blending of 87%, implying that the source itself comprises 13% of the baseline light. So for this event, we place an upper constraint on an MS mass based on the lens contributing no more than 18% (=31% − 13%) of the baseline light instead of the 87% found by just fitting the parallax model. We weight each solution by $\exp(-\Delta\chi^2/2)$ and find relative likelihoods of MS:WD:NS:BH = 31:19:14:37. Nearly all the BH probability is from disk lenses and bulge sources. This combination accounts for only about 37% of the total likelihood.

MACHO-98-BLG-6 has two solutions, but the second has little weight, $\exp(-\Delta\chi^2/2) = 3\%$. We find $\Delta\chi^2$-weighted relative likelihoods of MS:WD:NS:BH = 58:26:13:2. As in the previous event, the BH probability is from disk lenses and bulge sources. This combination of source and lens locations makes up only 21% of the likelihood for this event.

MACHO-99-BLG-22 is a strong BH candidate with relative likelihoods of MS:WD:NS:BH = 11:4:7:78. Unlike the previous two events, the BH probability is dominated by bulge-bulge lensing. This is due to its unusually large $\tilde{r}_E = 30$ AU and high $\tilde{v} = 83$ km s^{-1}.

Of course, these likelihood ratios depend on the priors embedded in the assumed MF. In particular, if the fraction of BHs in this MF were increased, the BH likelihood would rise correspondingly. However, if the prior on the BH fraction were altered within a plausible range, it would not materially affect the interpretation of MACHO-98-BLG-6. That is, even if the assumed density of BHs were doubled, this would only increase the BH likelihood of\kern 1pt MACHO-98-BLG-6 from 2% to 4%. However, if this density were cut in half, this would decrease the BH likelihood of MACHO-99-BLG-22 from 78% to 64% and of MACHO-96-BLG-5 from 37% to 22%.

Smith et al. (2005) examine these three events and find that MACHO-99-BLG-22 and MACHO-96-BLG-5 are inconsistent with their simulation, which does not include stellar remnants (see their Fig. 12). Event MACHO-98-BLG-6 is consistent with their simulation. Their results are compatible with our likelihood analysis.
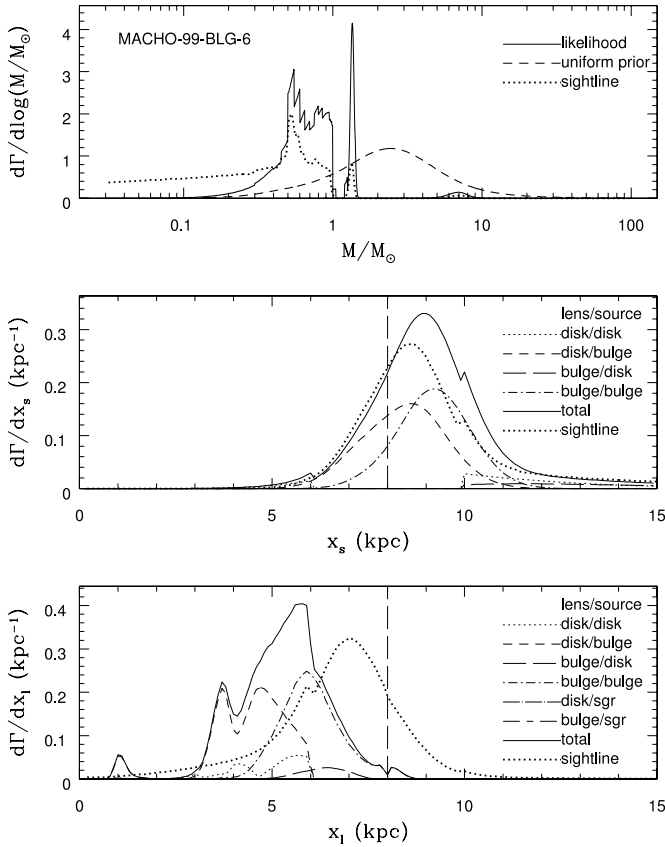
FIG. 6.—Relative likelihoods vs. mass, lens distance, and source distance for MACHO-98-BLG-6. In the top panel, the solid line is the result of our likelihood mass calculations. The dotted line is the expected distribution along this sight line from our model. The dashed line is the mass likelihood with a uniform prior in logarithmic mass. The middle and bottom panels give the likelihood of the source and lens distances, respectively.

4.4. Free-Floating Planet Candidate

OGLE-2003-BLG-84 reaches a peak magnification $A_{max} \sim 10$. We therefore incorporate finite-source effects into the fit and find an improvement $\Delta\chi^2 = 8.81$ for $\rho \equiv \theta_*/\theta_E = 0.107 \pm 0.030$, where θ_* is the angular size of the source. The source star has a baseline magnitude $I = 20.3$ with essentially no blending. Although we do not have a color-magnitude diagram of the field, this apparent magnitude is generally consistent with an upper MS star in the Galactic bulge. Hence, in fitting for finite-source effects, we use a solar linear limb-darkening coefficient (on the Albrow et al. [1999] system) $\Gamma_I = 0.3677$, and we estimate $\theta_* = r_\odot/R_0 = 0.58 \pm 0.07$ μas. This implies $\theta_E = \theta_*/\rho = 5.4 \pm 1.7$ μas. The best-fit parallax when finite-source effects are included is hardly changed, $\pi_E = 0.65 \pm 0.15$, or $\tilde{r}_E = 1.54 \pm 0.39$ AU. Combining the measurements of θ_E and π_E yields

$$M = \frac{\tilde{r}_E \theta_E}{\kappa} = 1.0 \pm 0.4 \times 10^{-3} \; M_\odot,$$
$$\pi_{rel} = \pi_E \theta_E = 3.5 \pm 1.3 \; \mu\text{as}. \qquad (21)$$

The implied Jupiter-like mass would be very exciting if true. However, the fact that this is only a 3 σ detection implies that caution is warranted. The conjointly derived relative parallax measurement is extremely small, implying a lens-source separation of only $D_{LS} = 224$ pc(D_S/R_0), where D_S is the distance to the source and $R_0 = 8$ kpc is the Galactocentric distance. Such a small source-lens separation is a priori unlikely but cannot be
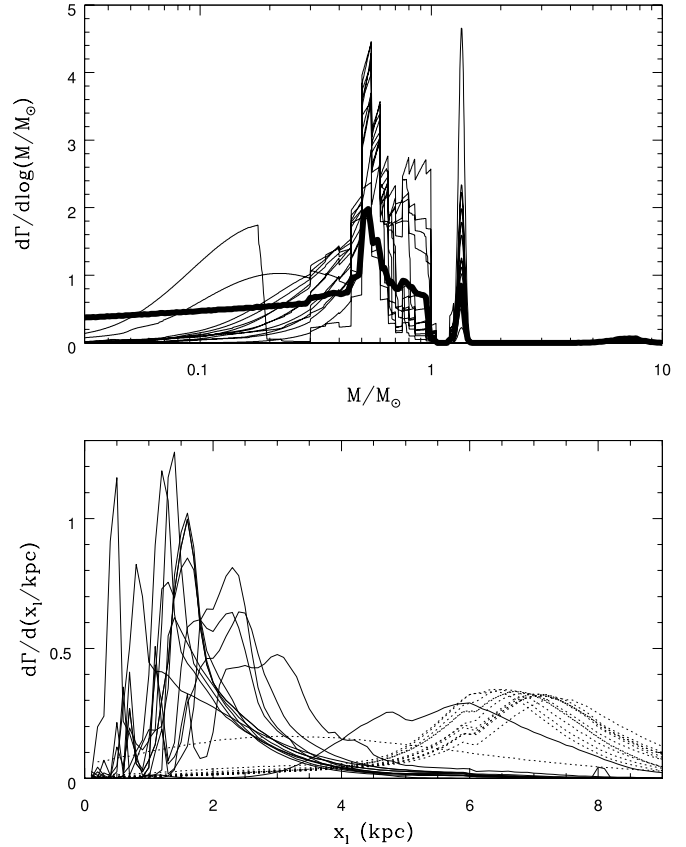
FIG. 7.—Relative likelihood of all 12 non–(BH/brown dwarf/planet/xallarap) events from this paper. The thick line in the top panel is our adopted MF prior. The bottom panel also shows the relative likelihoods for the same events, but vs. lens distance. The dotted lines are the expected distribution of events from our Galactic model in the same directions as these observed events. These composite plots illustrate how these parallax events have lenses that are closer and more massive than average.

strongly argued against on those grounds. This is because almost the only events that can give rise to both significant parallax and finite-source effects are those with very small θ_E and fairly small $\tilde{r}_E$. These criteria already imply very small (i.e., planetary) masses and generally small π_{rel}. Hence, while the characteristics of this event are intrinsically unlikely for an event chosen at

TABLE 3
LIKELIHOOD

Lens	Source	MS	WD	NS	BH	Total
MB104C: Solution 1, Weight 0.25						
Disk......................	Disk	1.89	0.64	0.06	0.00	2.59
	Bulge	17.43	9.78	1.12	0.04	28.37
	Sgr	0.45	0.19	0.01	0.00	0.65
	All	19.77	10.61	1.19	0.04	31.60
Bulge.....................	Disk	0.12	0.00	0.00	0.00	0.12
	Bulge	0.52	0.00	0.00	0.00	0.52
	Sgr	0.07	0.00	0.00	0.00	0.07
	All	0.70	0.00	0.00	0.00	0.70
Both......................	Disk	2.00	0.64	0.06	0.00	2.71
	Bulge	17.95	9.78	1.12	0.04	28.89
	Sgr	0.51	0.19	0.01	0.00	0.71
	All	20.47	10.61	1.19	0.04	32.30

NOTES.—Table 3 is published in its entirety in the electronic edition of the *Astrophysical Journal*. A portion is shown here for guidance regarding its form and content.

random, they are "normal" for an event with measured θ_E and $\tilde{r}_E$.

The xallarap analysis ($\Delta\chi^2_{\text{xallarap}} = 3.88$) of the event strongly confirms that parallax is the dominant contributor to the light-curve distortions. Under the assumption that the lens is indeed a planet, this can be used to place a rough lower limit on the planet's orbital distance a_{planet} from a possible host star. We assume that the light-curve distortion from the planet's acceleration is less than $\frac{1}{4}$ of the contribution from the Earth's motion; otherwise, the xallarap solution would be pushed away from the Earth parameters. However, since $D_S/D_L \sim 8$ kpc/224 pc ~ 36, the effect of the planet's acceleration on the light curve is effectively multiplied 36 times. Hence, the acceleration of the planet must be $4 \times 36 = 144$ times smaller than that of the Earth. This implies a semimajor axis $a_{\text{planet}} > 12$ AU$(M_*/M_\odot)^{1/2}$, where M_* is the mass of the host star.

While there is some evidence that this event is caused by a free-floating planet or by a planet at very wide separation from its parent star, there is no clear way to confirm this conclusion. First, the inference that there are finite-source effects rests on a relatively low $\Delta\chi^2$. Second, there are no independent data sets that could confirm this measurement. Finally, there is no way to independently verify that there is a free-floating planet at a distance $D_L \sim 8$ kpc. On the other hand, if the planet is bound to a star at wide (but not too wide) separation, then the star itself may eventually give rise to a second bump in the light curve. Unfortunately, the characteristics of this bump cannot be accurately predicted. If the star is, say, $0.3\,M_\odot$, then the stellar Einstein radius would be about 17 times larger than that of the planet, so one might then expect the heliocentric timescale to be 17 times longer than the $t_E \sim 430$ days found for the lens. However, if the planet were orbiting at 5 km s^{-1}, this would produce a difference in projected velocities of about $(8000/226)(5$ km s$^{-1}) = 180$ km s^{-1} between the planet and star. Since the projected velocity of the lens is only 6 km s^{-1}, this would reduce the predicted stellar Einstein crossing time by a factor of $180/6 = 30$ from $17 \times 430 = 7310$ to 244 days. Thus, the stellar bump could occur a few years (i.e., a few Einstein timescales) after the planetary bump and be of similar duration to it. In any event, if this second bump does occur, it will confirm the planetary nature of the event. But absent of that, this "planet" must remain a candidate.

4.5. Brown Dwarf Candidate MACHO-179-A

The brown dwarf candidacy of MACHO-179-A rests primarily on its small projected Einstein radius, $\tilde{r}_E = 0.23 \pm 0.05$ AU. From equation (1), this implies a lens mass

$$M = \frac{\pi_{\text{rel}}}{\kappa\pi_E^2} \rightarrow 0.065\,M_\odot\,\frac{100\text{ pc}}{D_L}, \quad (22)$$

with an error of about 0.17 dex. In the last step, we have made the approximation that $D_L \ll D_S$, which is certainly true unless the source lies well in the foreground ($D_S \lesssim 500$ pc) or the lens is of extremely low mass ($M \lesssim 10^{-3}\,M_\odot$). Then, from the projected velocity $\tilde{v} = 26.6$ km s^{-1}, the proper motion is

$$\mu = \tilde{v}\frac{\pi_{\text{rel}}}{\text{AU}} \rightarrow 56\,\frac{\text{mas}}{\text{yr}}\frac{100\text{ pc}}{D_L} = 56\,\frac{\text{mas}}{\text{yr}}\frac{M}{0.065\,M_\odot}. \quad (23)$$

Hence, if the lens is a star ($M > 0.08\,M_\odot$) rather than a brown dwarf, it is quite close ($D_L \lesssim 80$ pc) and has an extremely high proper motion, $\mu \gtrsim 69$ mas yr^{-1}. Such a star should be quite easy

to spot. For example, even extreme red dwarfs ($M \gtrsim 0.08\,M_\odot$) have $M_I \lesssim 14$, and so $I \lesssim 18.5$. An old WD of $M = 0.6\,M_\odot$ and $M_I \sim 15$ would be at 10 pc and so quite bright, $I \sim 15$.

There are already significant constraints on any such lenses from the light curve. The baseline flux is $R = 19.6$, and the blending fraction is $\eta_b = 0.32 \pm 0.23$. Hence, the lens brightness is limited by $R_l \gtrsim 20$. This clearly rules out WDs and permits only the most extreme M dwarfs, with $M \lesssim 0.1\,M_\odot$. Even these could easily be found by direct CCD imaging of the field. The very high predicted proper motion of the lens guarantees that it could be unambiguously identified if it is luminous.

If this option is excluded by future observations, then there remain only four possibilities: the lens is a brown dwarf, an NS, or a BH, or the light-curve distortion is not due to parallax at all but to some other effect, most likely xallarap. We examine the three alternatives to a brown dwarf in turn.

A BH would lie at only 1 pc. It would have an angular Einstein radius $\theta_E \sim 0''.25$ and a proper motion of about $6''$ yr^{-1}. It should therefore have given rise to a substantial number of microlensing events both during the original MACHO observations and also during observations of this field by OGLE-III.

An NS would lie at 5 pc and have $\theta_E \sim 50$ mas. While fairly large, this would not be large enough to guarantee other microlensing events during the periods of observations. However, other effects might be observable, such as X-ray emission due to interactions of the NS with the interstellar medium.

Xallarap can easily produce distortions that are misinterpreted as due to parallax with small $\tilde{r}_E$. Indeed, the event OGLE-2002-BLG-100 also has a fairly small $\tilde{r}_E \sim 0.46$ AU, which, as we show in § 5, is misinterpreted xallarap. By contrast, the xallarap analysis for MACHO-179-A shows that the xallarap parameters closely mimic the Earth's orbital parameters, indicating that it is unlikely, but not impossible, that the light-curve distortions are due to xallarap.

Moreover, the xallarap interpretation would imply other, possibly observable effects. Because these parameters indicate a source-binary orbital period of 1 yr and a nearly edge-on inclination, the source should have an annual velocity semiamplitude of $v \sim (30$ km s$^{-1})q(1 + q)^{-2/3}$, where q is the ratio of the source companion mass to the total mass of the binary. Thus, unless the source companion is extremely light, it should be possible to test the xallarap hypothesis directly from radial velocity measurements, although the faintness of the source would make this quite difficult.

Finally, we note that if the lens is a brown dwarf, it may also be possible to directly image it in the infrared. This will of course depend on its luminosity, which falls rapidly with both increasing age and decreasing mass.

5. XALLARAP ANALYSIS

The parallax effect is not the only way that a microlensing light curve can be distorted. The source may be part of a binary in which the acceleration of the source is causing the observed light-curve asymmetry (Griest & Hu 1992; Han & Gould 1997; Paczyński 1997). This effect is often called "xallarap." For each of these events, we search the class of xallarap solutions in which the source is in a circular orbit and its companion is either not lensed or too faint to contribute to the light curve. We search periods from 215 to 515 days (in steps of 20 days), every possible phase, and every orbital inclination (both in steps of 5°). Additional periods are searched when the best-fit period is near the lower or upper limit of the range probed.

If the light-curve distortion is actually due to parallax rather than xallarap, we expect the best-fit xallarap solution to closely

mimic the parallax solution. That is, we expect the best-fit period to be the period of the Earth (1 yr), the best-fit phase to be the ecliptic longitude of the event (typically $\lambda = 270^\circ$ for bulge events), and the best-fit inclination to be the (complement of the) ecliptic latitude of the event (typically $-11^\circ \lesssim \beta_{ec} \lesssim -3^\circ$ for bulge events). There exists a perfect north-south latitude degeneracy when the sign of u_0 and $\pi_{E,N}$ are both changed simultaneously. Therefore, we use the degenerate solution with the opposite u_0 as a seed for the northern latitudes. We search phases corresponding to ecliptic longitudes $180^\circ \leq l_{ec} \leq 360^\circ$ since there is an exact degeneracy in the supplementary angles. Note that the expected improvement for allowing the three extra xallarap parameters is small, $\langle \Delta\chi^2 \rangle = 3$.

For four of the events, we find $\Delta\chi^2 < 2$ (see Table 1), thus clearly confirming the parallax interpretation. Conversely, three of the events have $\Delta\chi^2 > 27$, which is a strong indication that these light curves have been distorted by xallarap. Another seven events have $3 < \Delta\chi^2 < 9$. The remaining eight events have $10 < \Delta\chi^2 < 25$. Since only 3 extra degrees of freedom are introduced in the xallarap analysis, it is surprising to find so many large improvements in χ^2. The majority of these may be the result of small systematic effects in the data that are more closely modeled by invoking these extra parameters. One possible such "systematic effect" is a minor xallarap perturbation on a distortion that is predominately caused by parallax. That is, if the source of a parallax event were a member of a binary, the small resulting xallarap effect could perturb the parallax solution, pushing it slightly away from Earth-like parameters.

One way to examine the possible influence of xallarap is to consider how reasonable the parameters are from the parallax solution versus the xallarap solution. The Einstein ring size projected into the source plane $\hat{r}_E$ is related to $\tilde{r}_E$, the Einstein ring size in the observer plane inferred from the "parallax interpretation" of the event, by

$$\hat{r}_E = \frac{q}{(1+q)^{2/3}} \left[\frac{M_s}{M_\odot} \left(\frac{P}{\text{yr}} \right)^2 \right]^{1/3} \tilde{r}_E, \qquad (24)$$

where q is the mass ratio of the source binary, M_s is the mass of the source being lensed, and P is the source period. Note that the factor in front has a maximum plausible value of $2^{-2/3} = 0.63$, under the reasonable assumption that $q \leq 1$. Another way to check for xallarap is to obtain radial velocity measurements of the source to confirm or discount its binary nature. We now discuss individual events with $\Delta\chi^2 > 4$.

MACHO-96-BLG-5 has $\Delta\chi^2_{\text{xallarap}} = 12.68$, but the best solution has a period of 365 days with a phase and inclination very similar to Earth's parameters (i.e., parallax). This is because the xallarap improvement is quite small compared to the parallax improvement $\Delta\chi^2_{\text{parallax}} = 2107.86$. That is, xallarap effects are at most a minor perturbation on parallax, which predominates overwhelmingly.

MACHO-98-BLG-6 has $\Delta\chi^2_{\text{xallarap}} = 15.89$. The best solutions tend to clump around periods of 400 days, but there does exist a solution with $\Delta\chi^2_{\text{xallarap}} = 13.22$, whose period (365 days) and complement of inclination (-5°) both agree with the parallax solution and whose phase differs from the parallax solution by only 20°. Again $\Delta\chi^2_{\text{xallarap}} \ll \Delta\chi^2_{\text{parallax}} = 557.71$, meaning that xallarap is at most a minor perturbation.

MACHO-99-BLG-1 has $\Delta\chi^2_{\text{xallarap}} = 15.58$. The phase and inclination parameters have a lot of scatter among the best xallarap solutions, but they are clumped around the Earth's parameters.

The best periods are near 750 days. However, the parallax model improves on the standard model considerably ($\Delta\chi^2_{\text{parallax}} = 1639.02$). The best xallarap solution improves only a small fraction better than the parallax model. Therefore, we conclude that this event is not strongly affected by xallarap.

MACHO-99-BLG-8 has $\Delta\chi^2_{\text{xallarap}} = 14.72$ with parameters similar to Earth's. Again the $\Delta\chi^2_{\text{xallarap}} \ll \Delta\chi^2_{\text{parallax}} = 1190.30$. Therefore, we conclude that this event is not strongly affected by xallarap.

MACHO-179-A has a relatively small $\Delta\chi^2 = 8.76$ and its best-fitting solutions clump near the parallax solution. We tentatively conclude that this event is not strongly affected by xallarap. However, in view of the striking implications of the parallax interpretation, an additional investigation is warranted (see § 4.5).

MACHO-98-BLG-1 with $\Delta\chi^2_{\text{xallarap}} = 112.24$ is the strongest xallarap candidate of the events in this paper. All three parameters differ significantly from the parallax solution with best-fitting periods near 425 days.

MACHO-95-BLG-27 has $\Delta\chi^2_{\text{xallarap}} = 17.38$ with xallarap parameters inconsistent with Earth's. The xallarap solutions strongly favor periods near 410 days and inclinations ~45°. Also the xallarap χ^2 improvement is significant relative to the parallax improvement over the standard model ($\Delta\chi^2_{\text{parallax}} = 190.69$). We conclude that this event is strongly affected by xallarap.

MACHO-99-BLG-22 has $\Delta\chi^2_{\text{xallarap}} = 4.28$. While the xallarap solutions do have periods near 365 days, the inclination parameters tend toward face-on solutions. The phase is not determined well from the fits. Again the $\Delta\chi^2_{\text{xallarap}} \ll \Delta\chi^2_{\text{parallax}} = 640.30$. We conclude that this event is not strongly affected by xallarap.

OGLE-1999-BLG-19 has $\Delta\chi^2_{\text{xallarap}} = 19.75$, but all the best solutions have parameters very close to the parallax parameters. Smith et al. (2002) also found that their xallarap model mirrored the Earth's orbital parameters. This is another case for which $\Delta\chi^2_{\text{xallarap}} \ll \Delta\chi^2_{\text{parallax}} = 10,506$, so this event is not strongly affected by xallarap.

OGLE-1999-CAR-01 has $\Delta\chi^2_{\text{xallarap}} = 5.13$ with parameters consistent with parallax. Therefore, we conclude that this event is not strongly affected by xallarap.

OGLE-2000-BLG-43 has $\Delta\chi^2_{\text{xallarap}} = 6.13$ and has orbital parameters consistent with Earth's, while $\Delta\chi^2_{\text{xallarap}} \ll \Delta\chi^2_{\text{parallax}} = 3519.65$. Therefore, this event is not strongly affected by xallarap.

The OGLE event sc33_4505 has $\Delta\chi^2_{\text{xallarap}} = 29.17$ and is a strong xallarap candidate. The best solutions have periods near 200 days. The xallarap solution clearly fits the data better as seen in Figure 8.

OGLE-2002-BLG-100 has $\Delta\chi^2_{\text{xallarap}} = 27.62$, which is substantial compared to $\Delta\chi^2_{\text{parallax}} = 139.38$. This event is likely affected by xallarap. The best solution has a period of 125 days, although the phase and inclination are consistent with those of the Earth. If the parallax solution were accepted at face value, its $\pi_E \sim 3$ would imply that the lens was a brown dwarf candidate, just as with MACHO-179-A. This has low prior probability but is not implausible. We should then also consider how plausible is the xallarap solution. First, we note that the parallax parameter in the best xallarap solution is $\pi_E \sim 0.3$ (compared to 3 in the parallax solution). Therefore, according to equation (24), the size of the Einstein ring projected on the source plane is $\hat{r}_E \sim 1.6q(1+q)^{-2/3}$ AU, which ranges from 0.15 to 1.0 AU for $0.1 < q < 1$. Note that $\hat{r}_E = 1$ AU implies $D_{LS} \simeq 122$ pc$(M_\odot/M)$, where $D_{LS} = D_L - D_S$ and where we have assumed $D_{LS} \ll D_S$. These masses and separations are fairly representative for bulge populations.
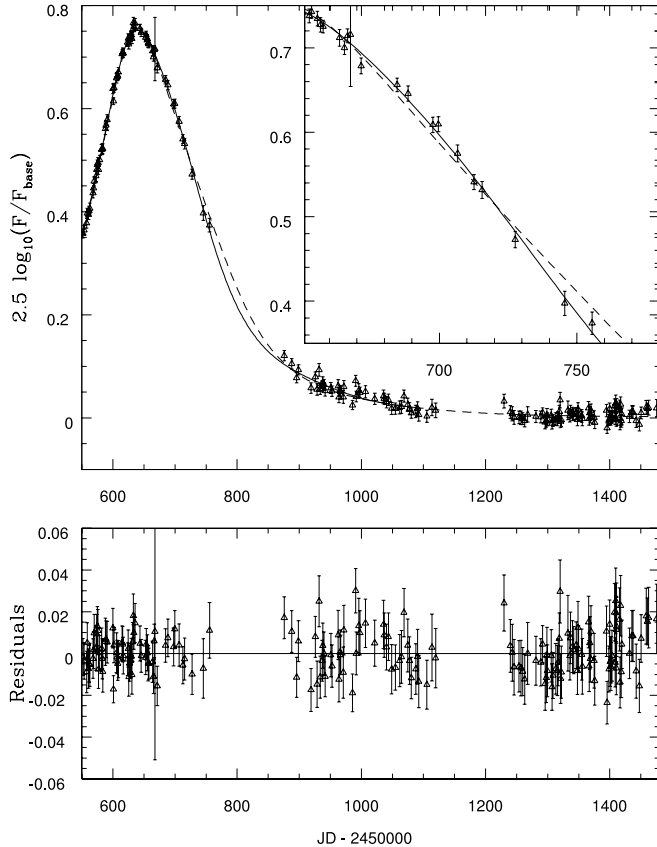
Fig. 8.—OGLE-II light curve of sc33_4505. The solid line is the best-fit xallarap model with $\Delta\chi^2_{\text{xallarap}} = 29.18$, and the dashed line is the best-fit parallax model. The inset in the top panel is an expanded view of the light curve that shows how the data better fit the xallarap model. The bottom panel shows the residuals of the xallarap model.

OGLE-2002-BLG-334 has $\Delta\chi^2_{\text{xallarap}} = 5.98$ and favors periods near 425 days and phases and inclinations inconsistent with parallax. The small $\Delta\chi^2_{\text{xallarap}}$ leads us to conclude that it is not strongly affected by xallarap, especially since $\Delta\chi^2_{\text{parallax}} = 612.88$. The differences must be due to systematic effects better modeled by the extra three parameters.

OGLE-2002-BLG-61 has $\Delta\chi^2_{\text{xallarap}} = 11.66$ and favors periods near 320 days with phases and inclinations inconsistent with parallax. This χ^2 improvement is significant relative to the parallax model's improvement over the standard model ($\Delta\chi^2 = 138.85$). Also, the best xallarap solutions have ~ 0 blending, which is more expected on this moderately bright event ($I_{\text{baseline}} = 17.4$). We conclude that this event is affected by xallarap.

OGLE-2003-BLG-188 has $\Delta\chi^2_{\text{xallarap}} = 8.21$ and favors periods near 440 days and inclinations inconsistent with parallax. However, the $\Delta\chi^2$ improvement is not very significant, and we have no clear reason to conclude that it is strongly affected by xallarap.

OGLE-2003-BLG-32 has $\Delta\chi^2_{\text{xallarap}} = 12.84$ and has orbital parameters consistent with Earth's. The improvement is minuscule compared to $\Delta\chi^2_{\text{parallax}} = 8042.12$, and so it is not strongly affected by xallarap.

6. DISCUSSION AND CONCLUSIONS

We have systematically studied 22 microlensing events with detectable parallax ($\Delta\chi^2 > 100$). We outlined a procedure that easily identifies the three discrete degeneracies known to affect microlensing parallax events. This procedure works provided that the geocentric reference frame is used. Surprisingly, we find 44 degenerate solutions among the 22 events in this paper. These degenerate solutions need to be considered even in events that appear to have a strong parallax detection. For example, event MACHO-104-C has a $\Delta\chi^2 = 1647.18$ parallax improvement over the standard microlensing model and we still find four highly degenerate solutions. Six of our events have $\Delta\chi^2 > 1000$ parallax improvements over the standard microlensing model. Only four of these have unique nondegenerate solutions (one of which is strongly affected by xallarap rather than parallax). We find no correlation between the number of degenerate solutions and either the ecliptic latitude or $\Delta\chi^2_{\text{parallax}}$.

We have reanalyzed three events previously identified as BH candidates and taken into account the newly identified solutions. We find that the lens of event MACHO-99-BLG-22 is a strong BH candidate, event MACHO-96-BLG-5 is a marginal BH candidate, and event MACHO-98-BLG-6 is a very weak BH candidate.

The adopted BH MF ($M \sim 7\,M_\odot$) is somewhat arbitrary and is based entirely on BHs found in binaries. Therefore, it is worthwhile to examine the higher mass candidates with a uniform prior in $\log M$ as shown in Figures 4–6 for the three BH candidates.

With this uniform prior we find that event MACHO-99-BLG-22 peaks at $M \sim 30\,M_\odot$, MACHO-96-BLG-5 is $M \sim 10\,M_\odot$, and MACHO-98-BLG-6 is $M \sim 2\,M_\odot$.

Figure 9 illustrates the difficulty of interpreting BH candidates from microlens parallax information alone. The line labeled "$[f(\mu_{\text{rel}})_{\text{disk}} + f(\mu_{\text{rel}})_{\text{bulge}}]x_l^4\pi_{\text{rel}}^5\phi(M)^{-1/2}$" represents the mass likelihood function under the assumption of a uniform $\log M$ prior (and restricted to bulge sources at $x_s = R_0$). Presumably a "typical" BH of mass $M = 7\,M_\odot$ would have event parameters that yield a peak in this line near $M = 7\,M_\odot$. However, MACHO-96-BLG-5 has a peak that lies above this value and yet is ranked only as a "marginal" (37%) candidate, while MACHO-98-BLG-6 has a peak somewhat below this value and yet is ranked as a "weak" (2%) candidate. That is, both events have parameters that are "typical" of actual BHs, yet neither is confirmed as such. Only MACHO-99-BLG-22, whose entire probability distribution is shifted sharply toward higher masses, survives as a strong candidate.

The problem is that the "typical" event parameters generated by BHs are also consistent with being generated by ordinary stars. Although this occurs with somewhat lower probability for any individual star compared to any individual BH, there are so many more stars than BHs (at least according to the model prior) that the stellar explanation will usually appear "most likely" even for genuine BH events. It is only the events whose parameters are indicative of such high masses that they are virtually inconsistent with any stellar-mass object that will survive as "strong candidates." Therefore, these strong candidates are either truly massive BHs ($M \gg 7\,M_\odot$) or ordinary ($M \sim 7\,M_\odot$) BHs that, by chance, happen to have extreme event parameters.

Thus, while microlens parallaxes can pick out BH candidates, to really find the true BHs and to measure their mass spectrum, it will be necessary to measure θ_E as well as π_E. For BHs, which are generally expected to have large θ_E, this may be possible using ground-based interferometers (Delplancke et al. 2001) but in any event can be done from space using the *Space Interferometry Mission* (Gould & Salim 1999).

Further measurements could help confirm the nature of these BH candidates. If we hypothesize that the lens of MACHO-96-BLG-5 is a BH of $7\,M_\odot$, then we know from the parallax fit that the lens is in the near disk. These assumptions yield a prediction
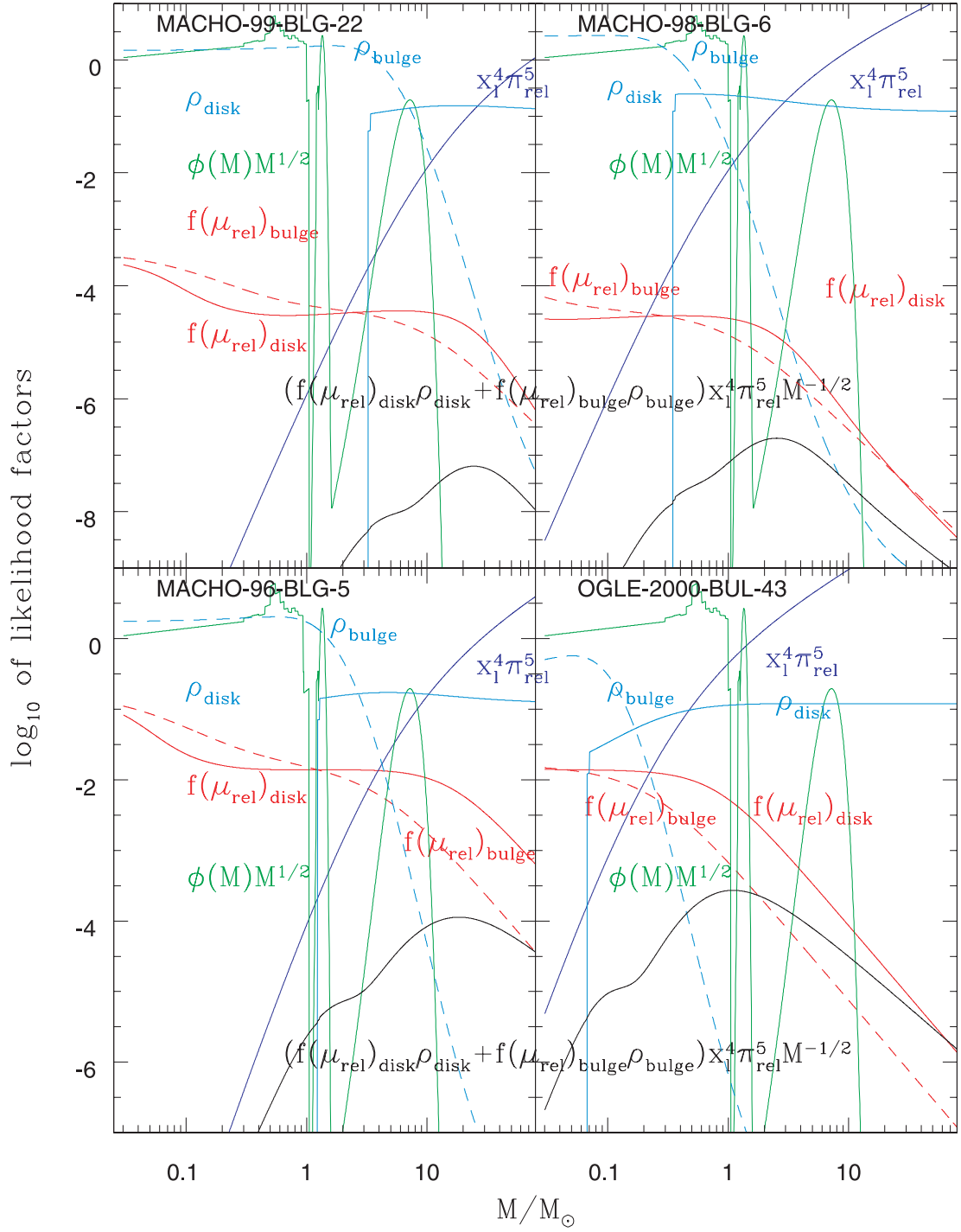
FIG. 9.—How the various likelihood factors affect the mass determination. For simplicity, we have only plotted these factors for a bulge source at 8 kpc while our full likelihood calculations (§ 4) are based on an integral over source distances. Hence, the figure only takes account of disk and bulge lenses on our side of the Galactic center. Shown here are the three BH candidates identified in Bennett et al. (2002), plus one other "normal" parallax event (OGLE-2000-BUL-43). Only the lowest $\Delta\chi^2$ solution is displayed for each of these events. The black line gives the likelihood for a uniform log mass prior.
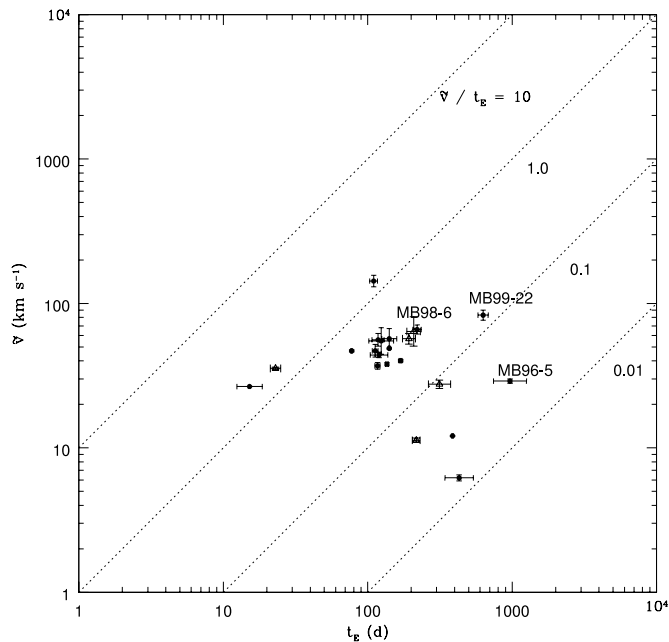
FIG. 10.—Projected velocity $\tilde{v}$ vs. heliocentric timescale $t_{\rm E}$ for the best solutions of all events in this paper. The open triangles represent xallarap candidates, while filled circles represent parallax events. This plot mirrors Fig. 9 of Smith et al. (2005), in which the four diagonal lines indicate constant $\tilde{v}/t_{\rm E} = \tilde{r}_{\rm E}/t_{\rm E}^2 = 10.0, 1, 0.1,$ and 0.01 km s^{-1} day^{-1}. These represent increasingly stronger parallax deviations.

We find that this sample of parallax events are biased toward lenses that are heavier [10] and closer than average. This is because it is easier to detect parallax from long-timescale events. Closer lenses give rise to slower $\tilde{v}$, which increases the timescale of the events. More massive lenses also give rise to longer timescales. We conclude that five of these events (23%) are strongly affected by xallarap rather than parallax.

Figure 10 shows the projected velocity $\tilde{v}$ versus the heliocentric timescale $t_{\rm E}$ of the best solutions of all events from this paper. The xallarap events (*open triangles*) are not distinguished from ordinary parallax events (*filled circles*) by these parameter measurements. This figure is consistent with the predictions of Figure 9 in Smith et al. (2003), which shows the distribution of simulated parallax events.

We find two additional interesting events. Event OGLE-2003-BLG-94 is a free-floating planet candidate. However, this is based on a 3 σ finite-source detection and there is no clear way to confirm this conclusion. Event MACHO-179-A is a brown dwarf candidate with a possibility of direct imaging in the infrared.

for the proper motion of the source, which could be confirmed or denied with *HST* data. However, there are several sources of uncertainty: the mass of the BH, the distance to the source, the velocity dispersions in the disk and bulge, and the fact that the microlens parallax is measured to only finite precision. This technique could be applied to other BH candidates as well.

[10] We conclude that we have not induced a selection bias by choosing events with geocentric timescales $t_{\rm E} > 60$ days for two reasons. First, events with shorter timescales are not expected to have $\Delta\chi^2 > 100$ because the Earth's velocity changes little in this time. Second, no events are known to have a parallax detection with both $\Delta\chi^2 > 100$ and $t_{\rm E} < 60$ days. Fig. 10 shows two events with heliocentric timescales less than 60 days, but in both cases their geocentric timescale (the quantity used to select events for further investigation) exceeds this cut.

REFERENCES

Afonso, C., et al. 2003, A&A, 404, 145
Agol, E., Kamionkowski, M., Koopmans, L. V. E., & Blandford, R. D. 2002, ApJ, 576, L131
Albrow, M. D., et al. 1999, ApJ, 522, 1022
Alcock, C., et al. 1993, Nature, 365, 621
———. 1995, ApJ, 454, L125
———. 1997a, ApJ, 474, 217
———. 1997b, ApJ, 486, 697
———. 2001, ApJ, 552, 582
An, J. H., et al. 2002, ApJ, 572, 521
Becker, A. C. 2000, Ph.D. thesis, Univ. Washington
Bennett, D. P., et al. 2002, ApJ, 579, 639
Bond, I., et al. 2001, MNRAS, 327, 868
Bragaglia, A., Renzini, A., & Bergeron, P. 1995, ApJ, 443, 735
Buchalter, A., & Kamionkowski, M. 1997, ApJ, 482, 782
Cavallo, R. M., Cook, K. H., Minniti, D., & Vandehei, T. 2003, Proc. SPIE, 4834, 66
Cox, A. N. 2000, Allen's Astrophysical Quantities (4th ed.; New York: Springer)
Cseresnjes, P., & Alard, C. 2001, A&A, 369, 778
Delplancke, F., Górski, K. M., & Richichi, A. 2001, A&A, 375, 701
Drake, A. J., Cook, K. H., & Keller, S. C. 2004, ApJ, 607, L29
Ghosh, H., et al. 2004, ApJ, 615, 450
Gould, A. 1992, ApJ, 392, 442
———. 2004, ApJ, 606, 319
Gould, A., Bennett, D. P., & Alves, D. R. 2004, ApJ, 614, 404
Gould, A., Miralda-Escudé, J., & Bahcall, J. N. 1994, ApJ, 423, L105
Gould, A., & Salim, S. 1999, ApJ, 524, 794
Griest, K., & Hu, W. 1992, ApJ, 397, 362
Han, C. 1998, ApJ, 500, 569
Han, C., & Gould, A. 1995, ApJ, 447, 53
———. 1996, ApJ, 467, 540

Han, C., & Gould, A. 1997, ApJ, 480, 196
———. 2003, ApJ, 592, 172
Holtzman, J. A., Watson, A. M., Baum, W. A., Grillmair, C. J., Groth, E. J., Light, R. M., Lynds, R., & O'Neil, E. J. 1998, AJ, 115, 1946
Ibata, R. A., Wyse, R. F. G., Gilmore, G., Irwin, M. J., & Suntzeff, N. B. 1997, AJ, 113, 634
Jaroszyński, M., et al. 2004, Acta Astron., 54, 103
Jiang, G., et al. 2004, ApJ, 617, 1307
Kamionkowski, M. 1995, ApJ, 442, L9
Kubas, D., et al. 2005, A&A, 435, 941
Mao, S. 1999, A&A, 350, L19
Mao, S., et al. 2002, MNRAS, 329, 349
Monaco, L., Bellazzini, M., Ferraro, F. R., & Bellazzini, M. 2004, MNRAS, 353, 874
Nemiroff, R. J. 1997, ApJ, 486, 693
Paczyński, B. 1986, ApJ, 304, 1
———. 1997, preprint (astro-ph/9711007)
Park, B.-G., et al. 2004, ApJ, 609, 166
Rhie, S. H., Becker, A. C., Bennett, D. P., Fragile, P. C., Johnson, B. R., King, L. J., Peterson, B. A., & Quinn, J. 1999, ApJ, 522, 1037
Smith, M. C., Belokurov, V., Evans, N. W., Mao, S., & An, J. H. 2005, MNRAS, 361, 128
Smith, M. C., Mao, S., & Paczyński, P. 2003, MNRAS, 339, 925
Smith, M. C., et al. 2002, MNRAS, 336, 670
Soszyński, I., et al. 2001, ApJ, 552, 731
Thorsett, S. E., & Chakrabarty, D. 1999, ApJ, 512, 288
Udalski, A. 2003, Acta Astron., 53, 291
Udalski, A., Szymański, M., Kałużny, J., Kubiak, M., Krzemiński, W., Mateo, M., Preston, G. W., & Paczyński, B. 1993, Acta Astron., 43, 289
Zoccali, M., Cassisi, S., Frogel, J. A., Gould, A., Ortolani, S., Renzini, A., Rich, R. M., & Stephens, A. W. 2000, ApJ, 530, 418